Search for $\eta_c(2S) \to \omega\omega$ and $\omega\phi$ and measurements of $\chi_{cJ} \to \omega\omega$ and $\omega\phi$ in $\psi(2S)$ radiative processes

M. Ablikim *et al.*[*]
(BESIII Collaboration)

(Received 13 August 2024; accepted 15 November 2024; published 6 February 2025)

Using $(2712 \pm 14) \times 10^6$ $\psi(2S)$ events collected with the BESIII detector at the BEPCII collider, we search for the decays $\eta_c(2S) \to \omega\omega$ and $\eta_c(2S) \to \omega\phi$ via the process $\psi(2S) \to \gamma\eta_c(2S)$. No statistically significant signals are observed. The upper limits of their product branching fractions at the 90% confidence level are determined to be $\mathcal{B}(\psi(2S) \to \gamma\eta_c(2S), \eta_c(2S) \to \omega\omega) < 1.04 \times 10^{-6}$ and $\mathcal{B}(\psi(2S) \to \gamma\eta_c(2S), \eta_c(2S) \to \omega\phi) < 1.85 \times 10^{-7}$, respectively. We also update the branching fractions of $\chi_{cJ} \to \omega\omega$ and $\chi_{cJ} \to \omega\phi$ via the $\psi(2S) \to \gamma\chi_{cJ}$ transition. Their branching fractions are determined to be $\mathcal{B}(\chi_{c0} \to \omega\omega) = (10.66 \pm 0.11 \pm 0.57) \times 10^{-4}$, $\mathcal{B}(\chi_{c1} \to \omega\omega) = (6.43 \pm 0.07 \pm 0.31) \times 10^{-4}$, $\mathcal{B}(\chi_{c2} \to \omega\omega) = (8.75 \pm 0.08 \pm 0.42) \times 10^{-4}$, $\mathcal{B}(\chi_{c0} \to \omega\phi) = (1.18 \pm 0.03 \pm 0.07) \times 10^{-4}$, $\mathcal{B}(\chi_{c1} \to \omega\phi) = (2.04 \pm 0.15 \pm 0.11) \times 10^{-5}$, and $\mathcal{B}(\chi_{c2} \to \omega\phi) = (9.58 \pm 1.07 \pm 0.76) \times 10^{-6}$, where the first uncertainties are statistical and the second are systematic.

DOI: 10.1103/PhysRevD.111.032001

I. INTRODUCTION

As bound states of $c\bar{c}$ pairs, charmonia are an ideal laboratory for testing the interplay between perturbative and nonperturbative quantum chromodynamics (QCD) [1]. Except for the J/ψ and $\psi(2S)$ states, charmonium states below the open charm production threshold, such as the P-wave state h_c, the S-wave ground state $\eta_c(1S)$, its first radial excitation $\eta_c(2S)$, and the P-wave states χ_{cJ} ($J = 0$, 1, 2), are not fully understood.

The decays of $\eta_c(1S)$ and $\eta_c(2S)$ into VV, where V stands for a light vector meson, are expected to be suppressed by the helicity selection rule (HSR) [2–4]. However, the measured branching fractions of $\eta_c(1S) \to VV$ are typically of the order of 10^{-3} to 10^{-2}. Such large branching fractions imply that the perturbative description of $\eta_c(1S)$ decays is inadequate and that nonperturbative mechanisms may play a crucial role [5]. Various nonperturbative models, such as the intermediate meson exchange model [6] and the charmonium light Fock component admixture model [7], have been proposed. In Ref. [8], the authors exploited the $^3P_0$ quark-creation mechanism model to calculate the decay width of $\eta_c(1S)$ into vector meson pairs ($\phi\phi$, $\rho\rho$, $K^*\bar{K}^*$, $\omega\omega$, $\omega\phi$), and the obtained results are compatible with the experimental measurements.

In addition, the relative ratios $\Gamma(\eta_c(2S) \to VV)/\Gamma(\eta_c(1S) \to VV)$ are predicted to be around 19% in Ref. [8]. Other predictions for the relative rate $\mathcal{B}(\eta_c(2S) \to \text{l.h.})/\mathcal{B}(\eta_c(1S) \to \text{l.h.})$ have been made within the framework of perturbative QCD. Here, l.h. denotes the light hadron channel. One model suggests [9]

$$\frac{\mathcal{B}(\eta_c(2S) \to \text{l.h.})}{\mathcal{B}(\eta_c(1S) \to \text{l.h.})} \approx \frac{\mathcal{B}(\psi(2S) \to \text{l.h.})}{\mathcal{B}(J/\psi \to \text{l.h.})} \approx 12\%, \quad (1)$$

based on the assumption that the decays of J/ψ and $\psi(2S)$ into light hadrons proceed through valence $c\bar{c}$ annihilation into three gluons at a typical distance scale of $1/m_c$. An alternative analysis predicts

$$\frac{\mathcal{B}(\eta_c(2S) \to \text{l.h.})}{\mathcal{B}(\eta_c(1S) \to \text{l.h.})} \approx 1, \quad (2)$$

as the dominant decay dynamics of the $\eta_c(1S)$ and $\eta_c(2S)$ involve the annihilation of charmed quark pairs into two gluons [10]. Using the available experimental data, the authors of Ref. [11] examined the branching fraction ratios of $\eta_c(1S)$ and $\eta_c(2S)$ in several decay modes, and found that the values are different from both theoretical expectations, albeit with large uncertainties. In experiments, the Belle Collaboration determined the branching fraction of $\eta_c(1S) \to \omega\omega$ to be $(1.62 \pm 0.57) \times 10^{-3}$ [12]. And the BESIII Collaboration set the upper limit on the branching fraction of $\eta_c(1S) \to \omega\phi$ at the 90% confidence level (CL)

[*]Full author list given at the end of the article.

as 2.5×10^{-4} [13]. However, the $\eta_c(2S)$ decays into these two final states have not been studied yet.

On the other hand, the measured branching fractions of the $\chi_{cJ} \to VV$ decays [14] are significantly larger than the predictions based on perturbative QCD calculations [15]. Especially, the BESIII experiment observed the $\chi_{cJ} \to \omega\phi$ decays [14], which violate the HSR and are expected to be doubly OZI suppressed. Recently, the branching fractions of $\chi_{cJ} \to \omega\phi$ were updated using 448×10^6 $\psi(2S)$ events [16], in which the $\chi_{c0,c1} \to \omega\phi$ decays are confirmed and the $\chi_{c2} \to \omega\phi$ decay is reported with a statistical significance of 4.8σ. The mechanism behind this unexpectedly large branching fraction remains unclear and needs further investigation.

In 2009, 2012, and 2021, a data sample of $(2712 \pm 14) \times 10^6$ $\psi(2S)$ events has been collected by the BESIII experiment [17], providing a good opportunity to study the $\eta_c(2S)$ decays. In this study, we search for the $\eta_c(2S) \to \omega\omega$ and $\eta_c(2S) \to \omega\phi$ decays via the $\psi(2S) \to \gamma\eta_c(2S)$ process, with ω and ϕ mesons reconstructed through $\omega \to \pi^+\pi^-\pi^0$ and $\phi \to K^+K^-$, respectively. Using the same data sample, we update the branching fractions of $\chi_{cJ} \to \omega\omega$ and $\chi_{cJ} \to \omega\phi$ with improved precision. An additional dataset recorded at the center-of-mass energy of 3.65 GeV is utilized to determine the contributions from the continuum processes.

II. BESIII DETECTOR AND MONTE CARLO SIMULATION

The BESIII detector [18] records symmetric e^+e^- collisions provided by the BEPCII storage ring [19] in the center-of-mass energy range from 1.84 to 4.95 GeV, with a peak luminosity of 1.1×10^{33} cm^{-2} s^{-1} achieved at $\sqrt{s} = 3.773$ GeV. The cylindrical core of the BESIII detector covers 93% of the full solid angle and consists of a helium-based multilayer drift chamber (MDC), a plastic scintillator time-of-flight system (TOF), and a CsI (Tl) electromagnetic calorimeter (EMC), which are all enclosed in a superconducting solenoidal magnet, providing a 1.0 T magnetic field. The solenoid is supported by an octagonal flux-return yoke with resistive plate chamber muon identifier modules interleaved with steel. The charged-particle momentum resolution at $1\ \mathrm{GeV}/c$ is 0.5%, and the $\mathrm{d}E/\mathrm{d}x$ resolution is 6% for the electrons from Bhabha scattering. The EMC measures photon energies with a resolution of 2.5% (5%) at 1 GeV in the barrel (end cap) region. The time resolution of the TOF barrel section is 68 ps, while that of the end cap section is 110 ps. The end cap TOF system was upgraded in 2015 with multigap resistive plate chamber technology, providing a time resolution of 60 ps, which benefits about 85% of the data used in this analysis [20].

Monte Carlo (MC) simulated data samples produced with a Geant4-based [21] software package, which includes the geometric description of the BESIII detector [22] and the detector response, are used to determine the detection efficiency and to estimate the background contributions. The simulation includes the beam energy spread and initial-state radiation (ISR) in the e^+e^- annihilations modeled with the generator KKMC [23]. The inclusive MC sample, which is used to study the background contribution, includes the production of the $\psi(2S)$ resonance, the ISR production of the J/ψ, and the continuum processes incorporated in KKMC [23]. All particle decays are modeled with EvtGen [24] using branching fractions either taken from the Particle Data Group (PDG) [25], when available, or otherwise estimated with LUNDCHARM [26]. Final state radiation from charged final state particles is incorporated with the PHOTOS package [27].

The exclusive decays $\psi(2S) \to \gamma X$ are generated according to the angular distribution $(1 + \lambda\cos^2\theta)$, where X refers to the $\eta_c(2S)$ or χ_{cJ} state, θ is the polar angle of the radiative photon in the rest frame of the $\psi(2S)$; the value of λ is set to 1 for the $\eta_c(2S)$, and to 1, $-1/3$, and $1/13$ for χ_{cJ} $(J = 0, 1, 2)$ [28], respectively. The $X \to \omega\omega$ and $X \to \omega\phi$ decays are generated using HELAMP [24], the helicity amplitude model where the angular correlation between the vector meson decays has been considered. Furthermore, two exclusive MC samples are generated to describe the background contributions, including $\psi(2S) \to \pi^0\pi^0 J/\psi$, $J/\psi \to \pi^+\pi^-\omega$ generated with the JPIPI [24] and phase space (PHSP) models and $\psi(2S) \to \omega K^+K^-$ generated with the PHSP model. The PHSP model represents the generic phase space for n-body decays, averaging over the spins of both initial and final states.

III. EVENT SELECTION

Candidate events for $\psi(2S) \to \gamma\eta_c(2S)$ with $\eta_c(2S) \to \omega\omega$ are required to contain at least five photons and four charged tracks, while candidate events for $\psi(2S) \to \gamma\eta_c(2S)$ with $\eta_c(2S) \to \omega\phi$ must contain at least three photons and four charged tracks. For each charged track, the distance of closest approach to the interaction point (IP) is required to be less than 10 cm along the z-axis (the symmetry axis of the MDC), and less than 1 cm in the plane perpendicular to the z-axis. The polar angle (θ) of the track must be within the fiducial volume of the MDC ($|\cos\theta| < 0.93$). Charged-particle identification (PID) is based on the combined information from the specific ionization energy loss in the MDC ($\mathrm{d}E/\mathrm{d}x$) and the flight time measured by the TOF, forming a $\chi^2_{\mathrm{PID}}(h)$ variable for each track, where h represents the charged-particle hypothesis (π, K, or p).

Photons are reconstructed from isolated showers in the EMC. The deposited energy of each shower is required to be at least 25 MeV in both barrel region ($|\cos\theta| < 0.80$) and end cap region ($0.86 < |\cos\theta| < 0.92$). To suppress electronic noise and showers unrelated to the event, the difference between the EMC time and the event start time is required to be within [0, 700] ns.

The π^0 candidate is reconstructed from a photon pair with an invariant mass satisfying $M_{\gamma\gamma} \in (0.10, 0.15)$ GeV$/c^2$. A one-constraint (1C) kinematic fit is performed to improve the energy resolution, constraining the invariant mass of the two photons to the nominal π^0 mass [25].

In the selection of $\psi(2S) \to \gamma\omega\omega$ candidate events, the four charged tracks are assumed to be pions. A six-constraint (6C) kinematic fit is applied, constraining the total reconstructed four-momentum to that of the initial state and the invariant masses of each photon pair to the nominal π^0 mass [25]. If there are additional photons and π^0 candidates in the event, the combination with the minimum χ^2_{6C} is chosen. To suppress the background, the results from a four-constraint (4C) fit are used, constraining only the total four-momentum. The requirement of χ^2_{4C} is optimized by maximizing the figure of merit (FOM) defined as $S/(3/2 + \sqrt{B})$ [29], where the number of 3 indicates three standard deviations, S and B are the numbers of signal and background events in the $\eta_c(2S)$ signal region $M_{2(\pi^+\pi^-\pi^0)} \in (3.60, 3.66)$ GeV$/c^2$, respectively. Here, S is calculated under the branching fraction assumption $\mathcal{B}(\eta_c(2S) \to \omega\omega) = \mathcal{B}(\eta_c(1S) \to \omega\omega)$ [25]; and B is estimated from the inclusive MC sample. The candidate events satisfying $\chi^2_{4C} < 15$ are kept. The two ω candidates with the minimum $(M^{(1)}_{\pi^+\pi^-\pi^0} - M_\omega)^2 + (M^{(2)}_{\pi^+\pi^-\pi^0} - M_\omega)^2$ are taken as the signal, where M_ω is the nominal ω mass [25]. The mass windows for both ω candidates are set as $M_{\pi^+\pi^-\pi^0} \in (0.737, 0.826)$ GeV$/c^2$, and they are randomly labeled. After these selections, no fake ω-pair peak is found in the MC simulation of the $\eta_c(2S) \to 2(\pi^+\pi^-\pi^0)$ decay. The distributions of $M^{(1)}_{\pi^+\pi^-\pi^0}$ versus $M^{(2)}_{\pi^+\pi^-\pi^0}$ for the signal MC simulation and data are shown in Fig. 1, where a clear $\omega\omega$ signal can be seen as indicated by the central red box. The peaking background events from the $\gamma\omega\pi^+\pi^-\pi^0$ and $\gamma 2(\pi^+\pi^-\pi^0)$ final states are evaluated with the sideband regions labeled by a, b, and c. These two peaking background contributions are referred to as the $\gamma\omega 3\pi$ and $\gamma 6\pi$ events in the following discussion. The method used to estimate the peaking background contributions will be introduced in Secs. IV and V.

In the selection of $\psi(2S) \to \gamma\omega\phi$ candidate events, the four charged tracks are assumed to be two pions and two kaons. A five-constraint (5C) kinematic fit is applied, constraining the total reconstructed four-momentum to that of the initial state (4C) and the invariant mass of the $\gamma\gamma$ pair to the nominal π^0 mass [25]. We define $\chi^2 = \chi^2_{5C} + \sum_{i=1}^{2} \chi^2_{\rm PID}(\pi) + \sum_{i=1}^{2} \chi^2_{\rm PID}(K)$ as the sum of the χ^2 from the 5C kinematic fit and the χ^2 from PID for the π or K particle hypothesis. To determine the types of final state particles and to select the best combination when additional photons or π^0 candidates are found in an event, the combination with the minimum χ^2 is chosen, and additionally $\chi^2_{4C} < 17$ is required.

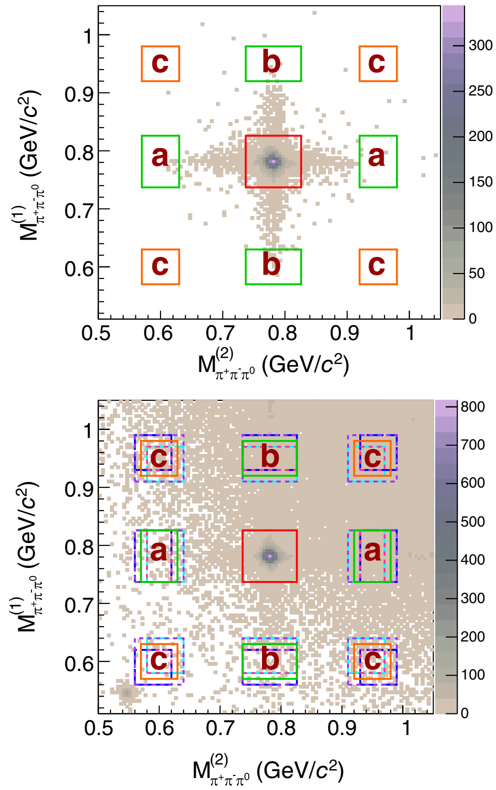

FIG. 1. Distributions of $M^{(1)}_{\pi^+\pi^-\pi^0}$ versus $M^{(2)}_{\pi^+\pi^-\pi^0}$ in the $\omega\omega$ mode for signal MC sample (top) and data (bottom). The red box represents the $\gamma\omega\omega$ signal region, the green boxes represents the $\gamma\omega\pi^+\pi^-\pi^0$ sideband regions (a) and (b), and the orange boxes represents the $\gamma 2(\pi^+\pi^-\pi^0)$ sideband regions (c). The cyan, blue, violet and pink dotted boxes in the bottom figure represent four alternative sideband regions used in the systematic uncertainty study (Sec. IV).

Similarly, the FOM is optimized under the branching fraction assumption $\mathcal{B}(\eta_c(2S) \to \omega\phi) = \mathcal{B}(\eta_c(1S) \to \omega\phi)$ [25] and the upper limit on the branching fraction of $\eta_c(1S) \to \omega\phi$ is used. The mass windows for the ω and ϕ candidates are set to be $M_{\pi^+\pi^-\pi^0} \in (0.737, 0.826)$ GeV$/c^2$ and $M_{K^+K^-} \in (1.005, 1.035)$ GeV$/c^2$, respectively. The distributions of $M_{\pi^+\pi^-\pi^0}$ versus $M_{K^+K^-}$ for the signal MC simulation and data are shown in Fig. 2, where the $\omega \to \pi^+\pi^-\pi^0$ and $\phi \to K^+K^-$ signals are clearly seen. The peaking background contributions from the $\gamma\pi^+\pi^-\pi^0\phi$, $\gamma\omega K^+K^-$, and $\gamma\pi^+\pi^-\pi^0 K^+K^-$ final states are evaluated with the sideband regions labeled by a, b, and c, and are referred to as the $\gamma\phi 3\pi$, $\gamma\omega 2K$, and $\gamma 3\pi 2K$ events, respectively.

Nonradiative decays $\psi(2S) \to VV$ can form a peak in the M_{VV} distribution around the $\eta_c(2S)$ mass. To suppress this peaking background, a modified kinematic fit is applied to the candidate events, where the energy of the radiative photon is allowed to vary in the fit (3C fit) and the obtained

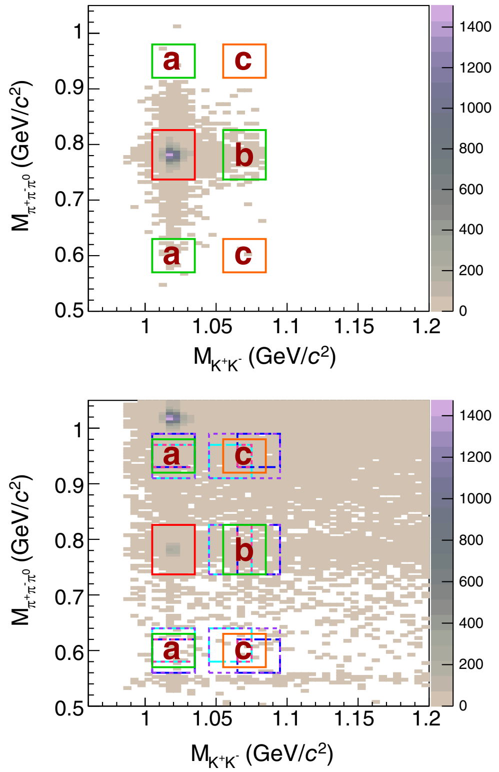

FIG. 2. Distributions of $M_{\pi^+\pi^-\pi^0}$ versus $M_{K^+K^-}$ in the $\omega\phi$ mode for signal MC sample (top) and data (bottom). The red box represents the $\gamma\omega\phi$ signal region, the green boxes represent the $\gamma\pi^+\pi^-\pi^0\phi$ (a) and $\gamma\omega K^+K^-$ (b) sideband regions, and the orange boxes represents the $\gamma\pi^+\pi^-\pi^0K^+K^-$ sideband regions (c). The cyan, blue, violet and pink dotted boxes in the bottom figure represent four alternative sideband regions used in the systematic uncertainty study (Sec. VI).

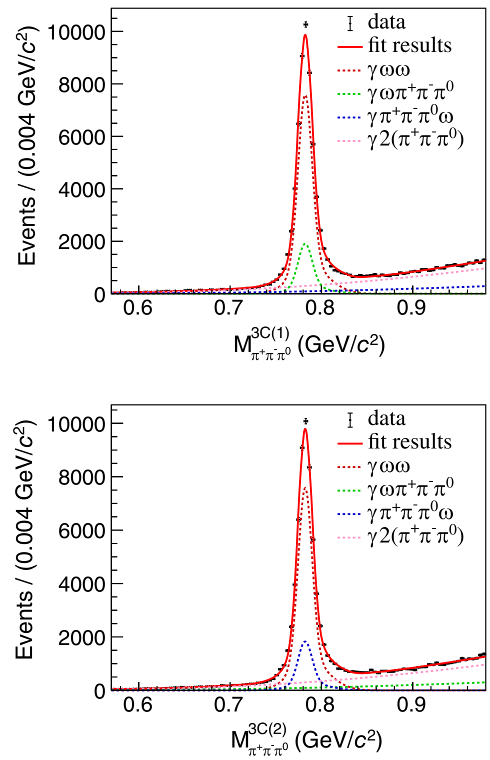

FIG. 3. Projections of the 2D fit to $M^{3C(1)}_{\pi^+\pi^-\pi^0}$ and $M^{3C(2)}_{\pi^+\pi^-\pi^0}$. The dots with error bars are data, the red solid lines are the fit results, the red dashed lines are the fits of the signal ($\gamma\omega\omega$) events, the green and blue dashed lines are the fits of the $\gamma\omega 3\pi$ events, and the pink dashed lines are the fits of the $\gamma 6\pi$ events.

invariant mass (M^{3C}_{VV}) distributions are used to extract the signal yields. The M^{3C}_{VV} distributions offer a resolution similar to the VV invariant mass from the 4C kinematic fit, but the background level is reduced since the nonradiative peak is shifted toward the $\psi(2S)$ mass region [30].

IV. BACKGROUND ESTIMATION

The study of the $\psi(2S)$ inclusive MC sample indicates that the dominant peaking background contributions in the M^{3C}_{VV} distributions come from $\psi(2S) \to \gamma\omega\pi^+\pi^-\pi^0$ and $\psi(2S) \to \gamma 2(\pi^+\pi^-\pi^0)$ for the $\omega\omega$ mode (referred to as $\gamma\omega 3\pi$ and $\gamma 6\pi$, respectively), and from $\psi(2S) \to \gamma\pi^+\pi^-\pi^0\phi$, $\psi(2S) \to \gamma\omega K^+K^-$, and $\psi(2S) \to \gamma\pi^+\pi^-\pi^0K^+K^-$ for the $\omega\phi$ mode (referred to as $\gamma\phi 3\pi$, $\gamma\omega 2K$ and $\gamma 3\pi 2K$, respectively). Several decay modes contribute in the $M^{3C}_{\omega\omega}$ and $M^{3C}_{\omega\phi}$ distributions as nonpeaking background events, with small contributions at the level of about 1.4%.

A. Peaking background

The peaking background contributions are estimated from the 2-dimensional (2D) sideband regions defined in Figs. 1 and 2, and the signal yields are extracted from the fits to the M^{3C}_{VV} distributions as discussed in Sec. V. The scale factors between the 2D signal and sideband regions are determined from a 2D fit to the 2D invariant mass distributions and calculated according to the integral of each components in the defined regions. In the 2D fit, the product of two double Gaussian functions is used to describe the VV signal events, a double Gaussian multiplied by a second-order polynomial is used to describe the events with only one V in the final state, and the product of two second-order polynomials is used to represent the events with no V resonance in the final state. The projections of the 2D fits on $M^{3C}_{\pi^+\pi^-\pi^0}$ and $M^{3C}_{\pi^+\pi^-\pi^0}/M^{3C}_{K^+K^-}$ are shown in Fig. 3 for the $\gamma\omega\omega$ mode and in Fig. 4 for the $\gamma\omega\phi$ mode in the region $(3.35, 3.60)$ GeV$/c^2$. The scale factors (f) for the events between the VV signal and sideband regions are summarized in Table I. The factors are determined separately for the three χ_{cJ} states. The M^{3C}_{VV} signal regions of χ_{c0}, χ_{c1}, and χ_{c2} states are defined as $(3.35, 3.47)$ GeV$/c^2$, $(3.47, 3.53)$ GeV$/c^2$, and $(3.53, 3.60)$ GeV$/c^2$, respectively.

B. $\psi(2S) \to \pi\pi J/\psi$

The fraction of the background events from $\psi(2S) \to \pi\pi J/\psi$ is approximately 1.0% for the $\gamma\omega\omega$ mode, primarily

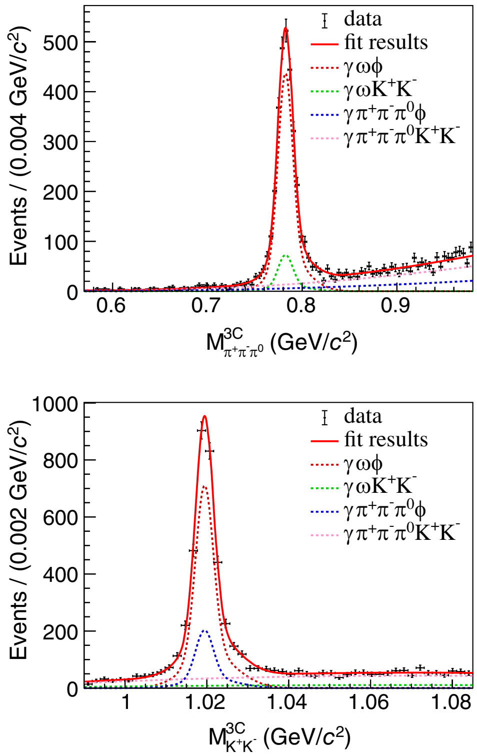

FIG. 4. Projections of the 2D fit to $M^{3C}_{\pi^+\pi^-\pi^0}$ and $M^{3C}_{K^+K^-}$. The dots with error bars are data, the red solid lines are the fit results, the red dashed lines are the fits of the signal ($\gamma\omega\phi$) events, the green and blue dashed lines are the fits of the $\gamma\omega 2K$ and $\gamma\phi 3\pi$ events, and the pink dashed lines are the fits of the $\gamma 3\pi 2K$ events.

stemming from $\psi(2S) \to \pi^0\pi^0 J/\psi$, and less than 0.4% for the $\gamma\omega\phi$ mode. By examining the recoil mass distributions of the $\pi\pi$ system in data, no distinct J/ψ peak is observed in the J/ψ mass region of $(3.05, 3.15)$ GeV$/c^2$. Since these events are smoothly distributed in the M^{3C}_{VV} distribution, no specific requirement is imposed to veto the minor contribution from $\psi(2S) \to \pi\pi J/\psi$. For the $\gamma\omega\omega$ mode, a dedicated $\psi(2S) \to \pi^0\pi^0 J/\psi$ MC sample is generated and the MC line shape is used to describe this background.

TABLE I. The scale factors (f) of each χ_{cJ} decay between the VV signal and sideband regions, where the uncertainties are statistical.

$\omega\omega$ mode	$\omega_1\pi^+\pi^-\pi^0$	$\pi^+\pi^-\pi^0\omega_2$	$2(\pi^+\pi^-\pi^0)$
f: χ_{c0}	0.554 ± 0.005	0.547 ± 0.005	0.303 ± 0.006
f: χ_{c1}	0.469 ± 0.003	0.471 ± 0.003	0.220 ± 0.003
f: χ_{c2}	0.447 ± 0.005	0.448 ± 0.006	0.200 ± 0.005
$\omega\phi$ mode	ωK^+K^-	$\pi^+\pi^-\pi^0\phi$	$\pi^+\pi^-\pi^0K^+K^-$
f: χ_{c0}	0.401 ± 0.005	0.684 ± 0.005	0.273 ± 0.005
f: χ_{c1}	0.510 ± 0.005	0.811 ± 0.005	0.413 ± 0.005
f: χ_{c2}	0.362 ± 0.005	0.628 ± 0.005	0.231 ± 0.005

C. Wrong $\gamma\omega\omega$ combinations

The $\psi(2S) \to \gamma\chi_{cJ}, \chi_{cJ} \to \omega\omega$ decays contaminate the $\eta_c(2S)$ signal region in case of a misassignment of the radiative photon. These events account for 61% of the background in the mass region $(3.60, 3.70)$ GeV$/c^2$. In Fig. 5(a) the comparison of the $M^{3C}_{\omega\omega}$ distributions between data and the three summed χ_{cJ} signals in the inclusive MC sample is illustrated. The inclusive MC line shape is used to describe this background in the fit to data.

D. $\psi(2S) \to \omega K^+K^-$

The fraction of the background events from $\psi(2S) \to \omega K^+K^-$ in the region $(3.60, 3.70)$ GeV$/c^2$ is 64% for the $\gamma\omega\phi$ mode, derived from the inclusive MC sample. The comparison of the $M^{3C}_{\omega\phi}$ distributions between data and the $\psi(2S) \to \omega K^+K^-$ MC sample is shown in Fig. 5(b). Around the $\psi(2S)$ peak, the distribution of data can be well described by the MC simulation. Therefore, the MC line shape is used to describe this background in the fit to data.

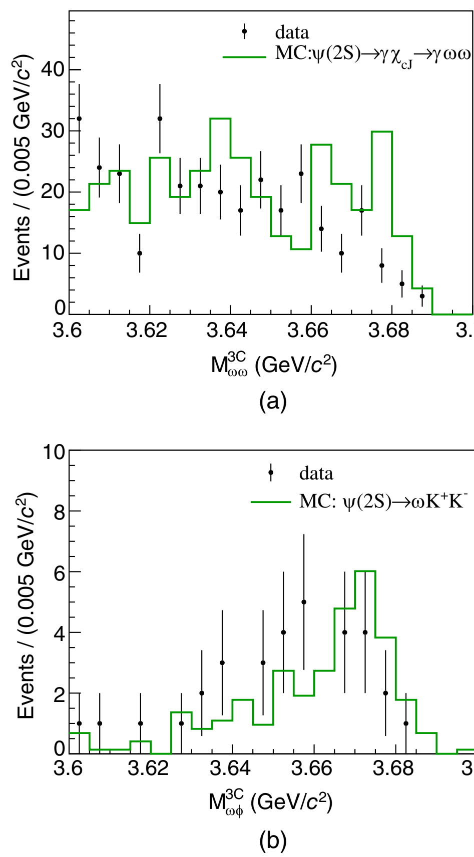

FIG. 5. (a) Comparison of the $M^{3C}_{\omega\omega}$ distributions between data (black dots with error bars) and $\psi(2S) \to \gamma\chi_{cJ}$ from the inclusive MC sample (green histogram); (b) Comparison of the $M^{3C}_{\omega\phi}$ distributions between data (black dots with error bars) and $\psi(2S) \to \omega K^+K^-$ from the signal MC sample (green histogram). (a) $\omega\omega$ mode. (b) $\omega\phi$ mode.

E. Continuum contribution

The background from the continuum processes is estimated using the data sample collected at the center-of-mass energy of 3.650 GeV. After applying the selection criteria, the contribution from surviving events is minimal. Considering the difference in production cross sections and integrated luminosities between the $\psi(2S)$ and continuum data samples, a scale factor of 9.48 is applied to the data sample at 3.650 GeV. The estimated numbers of continuum background events are 39 ± 20 for the $\gamma\omega\omega$ mode and 30 ± 17 for the $\gamma\omega\phi$ mode.

V. SIGNAL EXTRACTION

The number of signal events is extracted by an unbinned maximum likelihood fit of the M_{VV}^{3C} distributions within the range from 3.35 to 3.70 GeV$/c^2$, which includes the χ_{cJ} signals. Figures 6 and 7 display the M_{VV} distributions and the best fit results for the $\gamma\omega\omega$ and $\gamma\omega\phi$ modes, respectively, across the entire fit range and in the range only containing the $\eta_c(2S)$ signal. The χ^2/ndf values of the fits are $218.8/167 = 1.3$ for the $\gamma\omega\omega$ mode and $111.9/167 = 0.7$ for the $\gamma\omega\phi$ mode, where ndf is the number of degrees of freedom.

In the fit, the line shape of the $\eta_c(2S)$ is described by

$$[(BW(m) \times E_\gamma^3 \times f_d(E_\gamma)) \otimes DG \times \epsilon(m)] \otimes G, \quad (3)$$

where m represents M_{VV}^{3C}, $BW(m) = \frac{1}{2\pi} \cdot \frac{\Gamma}{(m-m_0)^2+\Gamma^2/4}$ is the Breit-Wigner function for the $\eta_c(2S)$ or χ_{cJ} resonance, with m_0 and Γ representing the mass and width fixed to individual PDG values [25]; $E_\gamma = \frac{M_{\psi(2S)}^2 - m^2}{2M_{\psi(2S)}}$ is the energy of the transition photon in the rest frame of $\psi(2S)$ [$M_{\psi(2S)}$ is the nominal mass of the $\psi(2S)$]; $f_d(E_\gamma) = \frac{E_0^2}{E_\gamma E_0 + (E_\gamma - E_0)^2}$ is the function to damp the diverging tail raised by E_γ^3, as used by the KEDR experiment [31] for a similar process, where $E_0 = \frac{M_{\psi(2S)}^2 - M_{\eta_c(2S)}^2}{2M_{\psi(2S)}}$ is the nominal energy of the transition photon; $DG = DG(m; m_1, \sigma_1, m_2, \sigma_2, r)$ is a double Gaussian function used to describe the mass resolution, and the parameters are estimated by using signal MC samples and fixed in the fit to data; $\epsilon(m)$ is the detection efficiency as a function of m, parametrized by fitting the efficiencies determined at each m using an ARGUS function multiplied by a polynomial [32]; $G = G(m; m_3, \sigma_3)$ is a single Gaussian function describing the difference of the mass resolution between data and MC simulation. For the χ_{cJ} signals, the parameters of the single Gaussian function are left free in the fit to data, while for the $\eta_c(2S)$ signal they are fixed to the values extrapolated from the values determined at the χ_{cJ} signals following a linear assumption, which are $m_3 = -1.85$ MeV$/c^2$ and $\sigma = 0.34$ MeV for the $\gamma\omega\omega$ mode; and $m_3 = -0.77$ MeV$/c^2$ and $\sigma = 1.31$ MeV for the $\gamma\omega\phi$ mode.

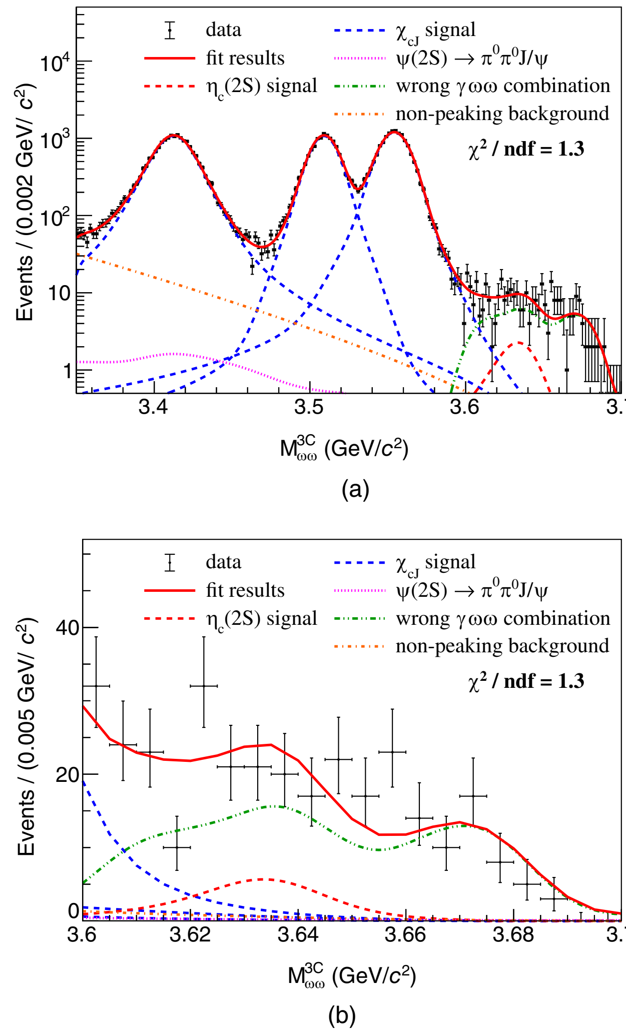

FIG. 6. The $M_{\omega\omega}^{3C}$ distributions in the whole fit range (a) and in the range only containing the $\eta_c(2S)$ signal (b). The dots with error bars are data, the red solid curves are the fit results, the blue dashed lines are the χ_{cJ} signal shapes, the red dashed lines are the $\eta_c(2S)$ signal shapes, the pink dotted line are the contributions from $\psi(2S) \to \pi^0\pi^0 J/\psi$, the green dashed lines are the background contributions from wrong $\gamma\omega\omega$ combinations (in which the radiative photon is misassigned), and the orange dotted lines are the nonpeaking background contributions.

For the $\gamma\omega\omega$ mode, three background components, $\psi(2S) \to \pi^0\pi^0 J/\psi$, $\psi(2S) \to \gamma\chi_{cJ}, \chi_{cJ} \to \omega\omega$, and nonpeaking background contributions, are included in the fit. The line shape and the number of background events of $\psi(2S) \to \pi^0\pi^0 J/\psi$ are fixed according to MC simulation and the branching fractions taken from the PDG [25]. The second component comes from $\psi(2S) \to \gamma\chi_{cJ}, \chi_{cJ} \to \omega\omega$, where the radiative photon is wrongly assigned. The line shape from the inclusive MC sample extracted with RooKeysPdf [33] is used. An additional ARGUS function is added in the fit to describe the nonpeaking background

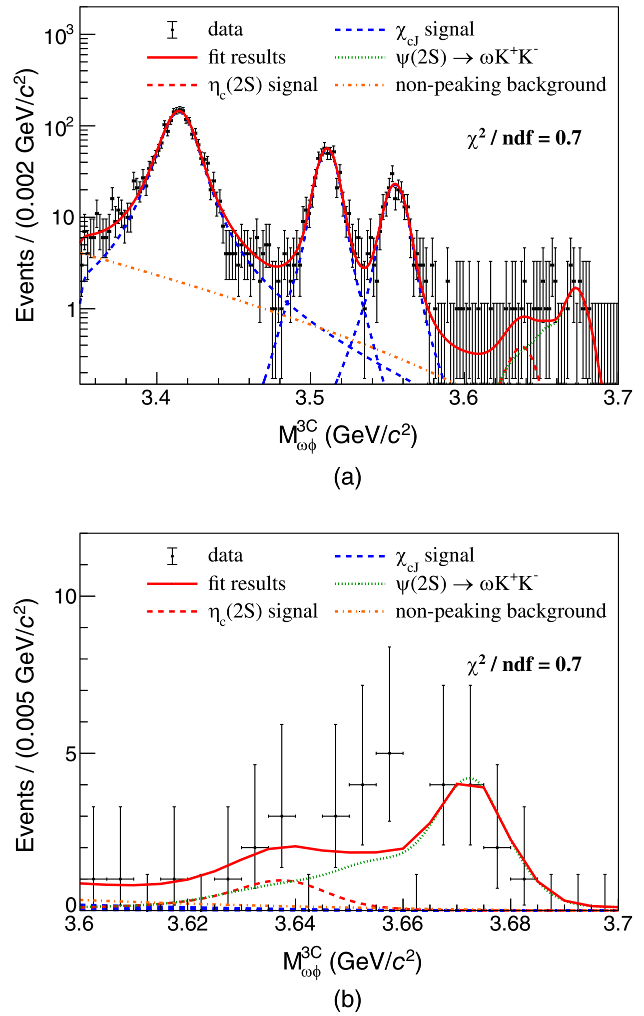

FIG. 7. The $M^{3C}_{\omega\phi}$ distributions in the whole fit range (a) and in the range only containing the $\eta_c(2S)$ signal (b). The dots with error bars are data, the red solid curves are the fit results, the blue dashed lines are the χ_{cJ} signal contributions, the red dashed lines are the $\eta_c(2S)$ signal shapes, the green dotted lines are the contributions from $\psi(2S) \to \omega K^+K^-$, and the orange dotted lines are the nonpeaking background contributions.

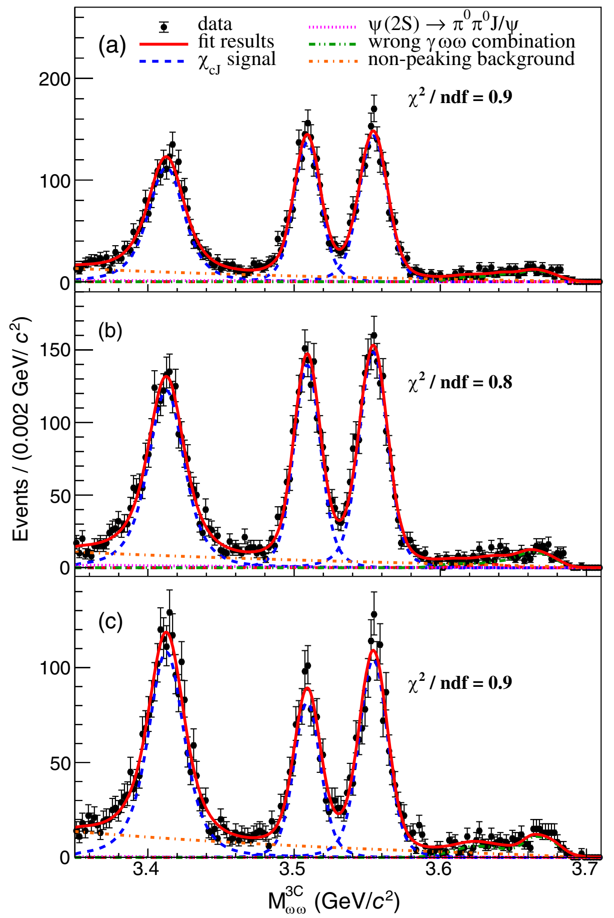

FIG. 8. The $M^{3C}_{\omega\omega}$ distributions in the sideband regions: (a) $\gamma\omega 3\pi$, (b) $\gamma\omega 3\pi$, and (c) $\gamma 6\pi$. The dots with error bars are data, the red solid curves are the best fit results, the blue dashed lines illustrate the χ_{cJ} signal shapes, the pink dotted lines represent the contribution from $\psi(2S) \to \pi^0\pi^0 J/\psi$, the green dot-dashed lines show the background contribution from wrong $\gamma\omega\omega$ combinations, and the orange dot-dashed lines are the nonpeaking background.

contribution from unknown processes. The yields of the second and third components are free in the fit. For the $\gamma\omega\phi$ mode, two background components are used: one to describe the $\psi(2S) \to \omega K^+K^-$ contribution, with the line shape fixed according to the MC simulation [25]; the other is an ARGUS function used to describe the smoothly distributed background events.

The peaking background contributions from $\chi_{cJ} \to \omega\pi^+\pi^-\pi^0$ and $\chi_{cJ} \to 2(\pi^+\pi^-\pi^0)$ for the $\gamma\omega\omega$ mode, and from $\chi_{cJ} \to \omega K^+K^-$, $\chi_{cJ} \to \pi^+\pi^-\pi^0\phi$, and $\chi_{cJ} \to \pi^+\pi^-\pi^0K^+K^-$ for the $\gamma\omega\phi$ mode, are estimated by using the events from the 2D sideband regions as shown in Figs. 3 and 4, respectively. The same formula as used for the VV signal region is adopted to fit the M^{3C}_{VV} distributions in the sideband regions. The fit results of the $\omega\pi^+\pi^-\pi^0$ and $2(\pi^+\pi^-\pi^0)$ contributions and of the ωK^+K^-, $\pi^+\pi^-\pi^0\phi$, and $\pi^+\pi^-\pi^0K^+K^-$ contributions are shown in Figs. 8 and 9, respectively.

The number of $\chi_{cJ} \to VV$ signal events ($N^{\rm net}_{\rm data}$) is calculated by

$$N^{\rm net}_{\rm data} = N^{\rm fitted}_{VV} - f_{(a)} \times N^{\rm fitted}_{(a)} - f_{(b)} \times N^{\rm fitted}_{(b)} + f_{(c)} \times N^{\rm fitted}_{(c)}, \qquad (4)$$

where $f_{\rm a,b,c}$ are the scale factors between the VV signal and sideband regions as listed in Table I, and $N^{\rm fitted}_{\rm a,b,c}$ are the numbers of events in the corresponding VV sideband regions. The obtained results are summarized in Table II.

The statistical significance is calculated from the difference of the logarithmic likelihoods [34], $-2\ln(\mathcal{L}_0/\mathcal{L}_{\rm max})$, where $\mathcal{L}_{\rm max}$ and $\mathcal{L}_0$ are the maximized likelihoods with and

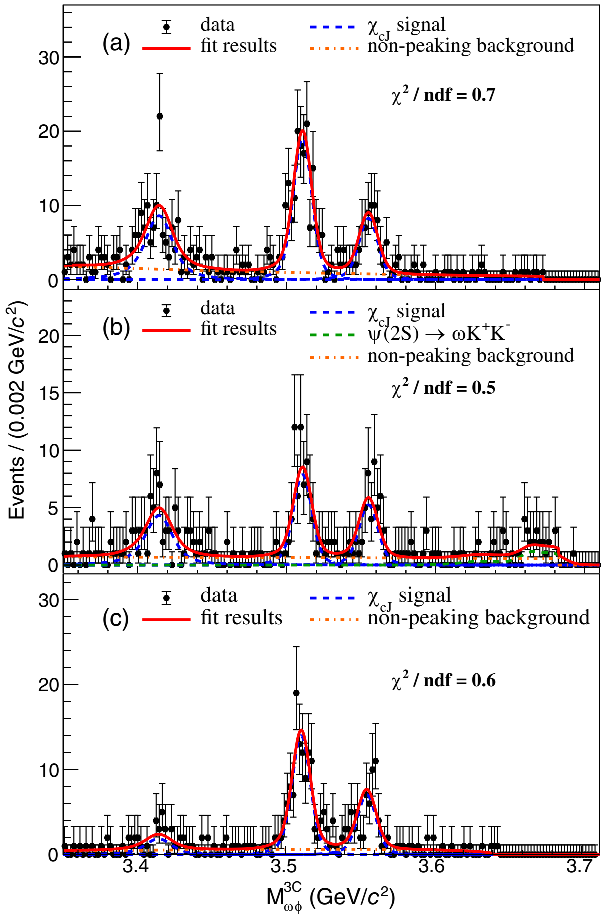

FIG. 9. The $M^{3C}_{\omega\phi}$ distributions in the sideband regions: (a) $\gamma\phi 3\pi$, (b) $\gamma\omega 2K$, and (c) $\gamma 3\pi 2K$. The dots with error bars are data, the red solid curves are the best fit results, the blue dashed lines show the χ_{cJ} signal shapes, the green dashed lines represent the contribution from $\psi(2S) \to \omega K^+K^-$, and the orange dot-dashed lines are the nonpeaking background.

without the signal component, taking into account the difference in the number of degrees of freedom. The statistical significances of $\eta_c(2S) \to \omega\omega$ and $\eta_c(2S) \to \omega\phi$ are 1.6σ and 1.2σ, with signal yields of 44 ± 26 and 6.0 ± 3.2, respectively. The decay $\chi_{c2} \to \omega\phi$ is observed with a statistical significance of 12.9σ.

An input/output check is performed using the inclusive MC samples to validate the fitting procedure. The output numbers determined from the fit are found to be consistent within one standard deviation with the input ones, indicating no bias.

We set the upper limits on the signal yields for $\eta_c(2S) \to \omega\omega$ and $\eta_c(2S) \to \omega\phi$ at the 90% CL with the likelihood scan method as shown in Fig. 10. For each signal decay, the upper limit of $N_{\rm sig}$ is determined by solving the equation $\int_0^{N_{\rm sig}} \mathcal{L}(x)dx / \int_0^{+\infty} \mathcal{L}(x)dx = 0.9$, where x is the assumed $\eta_c(2S)$ signal yield, and $\mathcal{L}(x)$ is the corresponding maximized likelihood of the fit.

VI. SYSTEMATIC UNCERTAINTY ESTIMATION

Table III summarizes the sources of systematic uncertainties, which are described in details as follows.

(i) *MDC tracking.* The systematic uncertainty of the π tracking is studied via the control sample $J/\psi \to \pi^+\pi^-\pi^0$ [35]. A 2D systematic uncertainty matrix is provided with 11 intervals along $P_T(\pi)$ and 10 intervals along $\cos\theta$. The systematic uncertainty of each pion track is determined using a weight method according to the $P_T(\pi)$ and $\cos\theta$ distributions in the signal MC process. The systematic uncertainty for kaon tracking is estimated to be 1.0% per K track using the control sample $J/\psi \to K^0_S K^\pm \pi^\mp$ [36].

(ii) *Photon reconstruction.* The photon detection efficiency is studied by using the control sample $e^+e^- \to \gamma\mu^+\mu^-$ in the photon energy region (0.1, 1.2) GeV.

(iii) *Mass window.* The systematic uncertainty from the π^0 mass window is assigned as the difference between the efficiencies of data and MC simulation caused by the $M_{\gamma\gamma}$ requirement. This uncertainty has been assigned as 1.0% by using the control sample of $J/\psi \to \pi^0 p\bar{p}$ [37].

The systematic uncertainties from the ω and ϕ mass windows are estimated by fitting the $M_{\pi^+\pi^-\pi^0}$ or $M_{K^+K^-}$ distributions in data and examing the mass resolution difference. The difference in the

TABLE II. The numbers of signal events for the χ_{cJ} in signal and sideband regions, where the uncertainties are statistical.

Channel	$N^{\rm fitted}_{\omega\omega}$	$N^{\rm fitted}_{\omega_1\pi^+\pi^-\pi^0}$	$N^{\rm fitted}_{\pi^+\pi^-\pi^0\omega_2}$	$N^{\rm fitted}_{2(\pi^+\pi^-\pi^0)}$	$N^{\rm net}_{\rm data}$
$\chi_{c0} \to \omega\omega$	19120 ± 171	2106 ± 59	1940 ± 57	1867 ± 56	17458 ± 178
$\chi_{c1} \to \omega\omega$	12993 ± 124	1644 ± 46	1612 ± 46	963 ± 40	11674 ± 128
$\chi_{c2} \to \omega\omega$	15678 ± 131	1894 ± 49	1832 ± 48	1331 ± 46	14276 ± 135
Channel	$N^{\rm fitted}_{\omega\phi}$	$N^{\rm fitted}_{\omega K^+K^-}$	$N^{\rm fitted}_{\pi^+\pi^-\pi^0\phi}$	$N^{\rm fitted}_{\pi^+\pi^-\pi^0K^+K^-}$	$N^{\rm net}_{\rm data}$
$\chi_{c0} \to \omega\phi$	1989 ± 50	58 ± 10	116 ± 14	25 ± 7	1893 ± 51
$\chi_{c1} \to \omega\phi$	468 ± 23	64 ± 9	156 ± 14	115 ± 12	356 ± 26
$\chi_{c2} \to \omega\phi$	198 ± 15	45 ± 8	70 ± 9	60 ± 9	151 ± 17

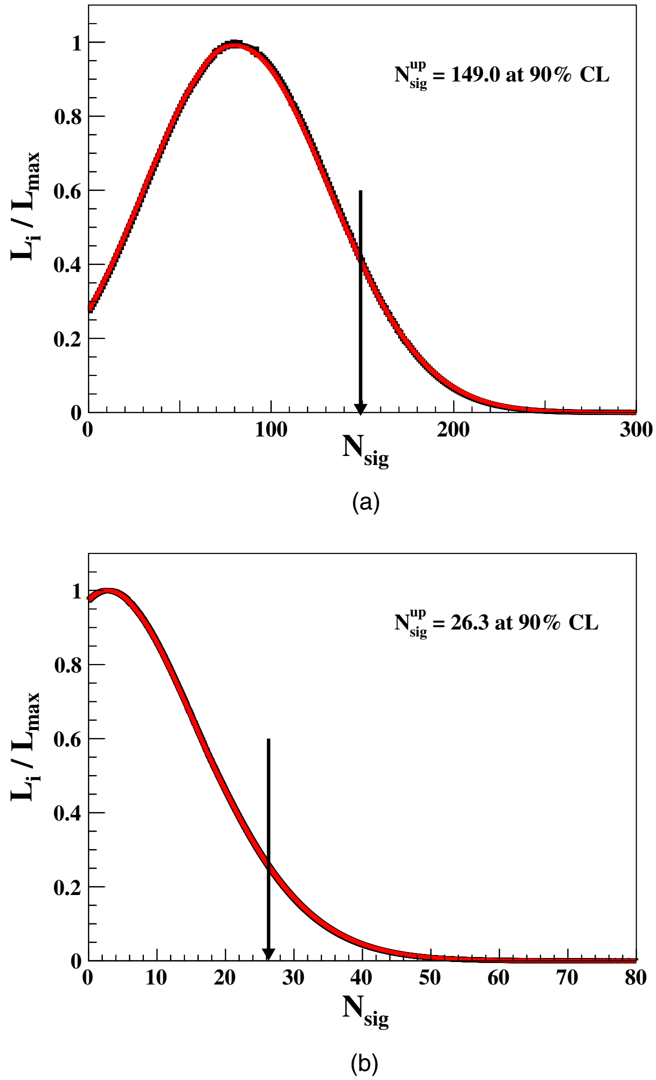

FIG. 10. Likelihood distributions as a function of the number of signal events for the two decay modes, where the black lines represent the likelihood distribution for data, and the red lines are the normalized likelihood distribution including the systematic uncertainties. (a) $\psi(2S) \to \gamma\eta_c(2S) \to \gamma\omega\omega$. (b) $\psi(2S) \to \gamma\eta_c(2S) \to \gamma\omega\phi$.

acceptance efficiencies for each mass window between data and MC simulation is taken as the systematic uncertainty.

(iv) *Kinematic fit.* The systematic uncertainty from the kinematic fit is estimated by correcting the helix parameters of the charged tracks in the MC simulation [38]. The differences in the detection efficiencies with and without correcting the helix parameters is taken as the uncertainty.

(v) *Helicity angle.* For the $\chi_{c1} \to \omega\omega$ decay, the $\cos\theta_\omega$ distributions differ between data and MC simulation. To take into account this difference into the uncertainty estimation, the $\cos\theta_\omega$ distributions are divided into 100 bins, and an averaged efficiency is calculated from the signal MC sample, by weighting the efficiency obtained for each bin by the fraction of generated events within that bin; in analogous way, the averaged efficiency is calculated for the data sample, by weighting the selected events using the bin-dependent efficiency obtained from signal MC sample. The difference between the averaged efficiencies for data and MC simulation is taken as the systematic uncertainty.

(vi) *Sideband.* The systematic uncertainty from the choice of the sideband regions is estimated by changing the ranges as shown in Figs. 1(b) and 2(b), and the maximum difference of the fitted signal yield is taken as the systematic uncertainty.

The scale factors listed in Table I are calculated with parameters fixed to the results from the 2D fit; the uncertainties introduced by the fit parameters are estimated by generating multidimensional Gaussian random numbers using the covariance matrix values from the fit as input. The standard deviation of the resultant number of the χ_{cJ} events is taken as the systematic uncertainty.

(vii) *Detection efficiency.* In the estimation of the detection efficiencies of the $\eta_c(2S) \to VV$ decays, the contribution from the 2D VV sideband regions is not considered. The change of the detection efficiency after considering the 2D VV sideband contributions is taken as the systematic uncertainty.

(viii) *Total number of $\psi(2S)$ events.* The total number of $\psi(2S)$ events in data is determined to be $(2712 \pm 14) \times 10^6$ [17]; and its relative uncertainty is 0.5%.

(ix) *Input branching fractions.* The systematic uncertainties from the branching fractions of $\psi(2S) \to \gamma X$ (where X is the χ_{cJ}), $\omega \to \pi^+\pi^-\pi^0$, $\phi \to K^+K^-$ and $\pi^0 \to \gamma\gamma$ decays are quoted from the PDG [25].

(x) *Damping function form.* An alternative damping function used by the CLEO Collaboration [39], $f_d(E_\gamma) = \exp(-E_\gamma^2/8\beta^2)$ where β is a free parameter, is chosen to estimate the related uncertainty. The difference in the fitted signal yields between the nominal and alternative damping functions is taken as the systematic uncertainty.

(xi) *Efficiency curve.* The efficiency curve is fitted by an ARGUS function multiplied by a polynomial. As an alternative choice, we describe the efficiency curve derived with RooHistPdf [40], and take the difference in the branching fraction with these two efficiency curves as the systematic uncertainty.

(xii) *MC resolution and detector resolution.* The systematic uncertainties related to the modeling of the MC resolution is estimated by using RooKeysPdf [33] to replace the double Gaussian resolution function. The change of the branching fraction is taken as the systematic uncertainty.

TABLE III. Systematic uncertainties (in %) for the branching fraction measurements.

Source	$\eta_c(2S)\to\omega\omega$	$\chi_{c0}\to\omega\omega$	$\chi_{c1}\to\omega\omega$	$\chi_{c2}\to\omega\omega$	$\eta_c(2S)\to\omega\phi$	$\chi_{c0}\to\omega\phi$	$\chi_{c1}\to\omega\phi$	$\chi_{c2}\to\omega\phi$
MDC tracking	0.5	0.4	0.5	0.4	2.2	2.2	2.2	2.2
Photon reconstruction	2.5	2.5	2.5	2.5	1.5	1.5	1.5	1.5
Mass window-π^0	2.0	2.0	2.0	2.0	1.0	1.0	1.0	1.0
Mass window-ω_1	0.0	0.0	0.0	0.0	⋯	⋯	⋯	⋯
Mass window-ω_2	0.0	0.0	0.0	0.0	⋯	⋯	⋯	⋯
Mass window-ω	⋯	⋯	⋯	⋯	0.0	0.0	0.0	0.0
Mass window-ϕ	⋯	⋯	⋯	⋯	0.1	0.1	0.1	0.1
Kinematic fit	1.8	1.5	1.5	1.7	3.1	2.6	2.9	2.6
Helicity angle	⋯	⋯	0.5	⋯	⋯	⋯	⋯	⋯
Sideband region	⋯	0.2	0.2	0.2	⋯	0.7	1.7	2.2
Sideband factor	⋯	0.0	0.1	0.1	⋯	0.1	0.3	0.5
Detection efficiency	0.7	⋯	⋯	⋯	1.4	⋯	⋯	⋯
Total number of $\psi(2S)$ events	0.5	0.5	0.5	0.5	0.5	0.5	0.5	0.5
$\mathcal{B}(\psi(2S)\to\gamma\chi_{cJ})$	⋯	2.0	2.5	2.1	⋯	2.0	2.5	2.1
$\mathcal{B}(\omega\to\pi^+\pi^-\pi^0)$	1.6	1.6	1.6	1.6	0.8	0.8	0.8	0.8
$\mathcal{B}(\phi\to K^+K^-)$	⋯	⋯	⋯	⋯	1.0	1.0	1.0	1.0
$\mathcal{B}(\pi^0\to\gamma\gamma)$	0.1	0.1	0.1	0.1	0.0	0.0	0.0	0.0
Damping function form	⋯	0.2	0.1	1.3	⋯	0.1	0.4	0.9
Efficiency curve	⋯	0.0	0.1	0.1	⋯	0.0	0.4	0.3
MC resolution	⋯	0.3	0.2	0.4	⋯	0.1	1.0	1.7
Resolution between data and MC	⋯	⋯	⋯	⋯	⋯	⋯	⋯	⋯
Continuum background	⋯	0.0	0.0	0.0	⋯	0.1	1.2	2.5
Shape of $\psi(2S)\to\pi^0\pi^0J/\psi$	⋯	0.0	0.0	0.0	⋯	⋯	⋯	⋯
Number of $\psi(2S)\to\pi^0\pi^0J/\psi$	⋯	0.0	0.0	0.0	⋯	⋯	⋯	⋯
Shape of inclusive MC	⋯	0.4	0.3	0.2	⋯	⋯	⋯	⋯
Shape of $\psi(2S)\to\omega K^+K^-$	⋯	⋯	⋯	⋯	⋯	0.0	0.4	0.3
ARGUS function	⋯	2.8	0.3	0.5	⋯	3.8	0.7	5.4
Total	4.1	5.4	4.8	4.8	4.6	6.1	5.6	7.9

The detector resolution difference between data and MC simulation for the $\eta_c(2S)$ signal is obtained by fitting the χ_{cJ} signals and extrapolating to the $\eta_c(2S)$ mass. The resolution difference for the line shape of the $\eta_c(2S)$ signal is varied by $\pm1\sigma$, and the largest variation of the branching fraction is taken as the systematic uncertainty.

(xiii) *Background shape.* The main background contributions are from continuum, $\psi(2S)\to\pi^0\pi^0J/\psi$ and $\psi(2S)\to\omega K^+K^-$. In the nominal fit, the continuum contribution is not included since it is very small. The change of the branching fraction after taking this contribution into account is taken as the systematic uncertainty.

The systematic uncertainty from the fixed $\psi(2S)\to\pi^0\pi^0J/\psi$ background yield is estimated by varying it within $\pm1\sigma$ of the quoted branching fractions [25], and refitting the M_{VV}^{3C} distributions. The uncertainties from the line shapes of $\psi(2S)\to\pi^0\pi^0J/\psi$ and $\psi(2S)\to\gamma\chi_{cJ},\chi_{cJ}\to\omega\omega$ for the $\omega\omega$ mode, and $\psi(2S)\to\omega K^+K^-$ for the $\omega\phi$ mode are estimated by changing RooKeysPdf [33] into RooHistPdf [40]. The uncertainty from the non-peaking background contribution is determined by replacing the ARGUS function with a 1st-order polynomial multiplied by a truncation function, which is used to set the PDF to zero in the mass region above 3.69 GeV$/c^2$ (as it exceeds the phase space). For each case, the difference in the signal yields is taken as the systematic uncertainty.

The systematic uncertainty on the upper limit of signal yield $N_{\rm sig}^{\rm up}$ at the 90% CL includes additive and multiplicative sources. The additive systematic uncertainty includes the damping function form, the efficiency curve, the MC resolution, the resolution difference between data and MC simulation, and the background shape. They are considered separately. For each decay and each case, the largest upper limit of the signal yield is selected. The sources of multiplicative systematic uncertainty are listed in Table III. It is incorporated by convolving a Gaussian function to the likelihood distribution in which the total multiplicative systematic uncertainty is taken as the standard deviation [41]. This is accomplished via

$$\mathcal{L}'(N)=\int_0^1\mathcal{L}\left(\frac{S}{\hat{S}}N\right)\exp\left[\frac{-(S-\hat{S})}{2\sigma_S^2}N\right]dS,\qquad(5)$$

TABLE IV. Net signal yields, detection efficiencies, and branching fractions of the $\chi_{cJ} \to \omega\omega$ and $\chi_{cJ} \to \omega\phi$ decays. The branching fractions of χ_{cJ} from the world average values [25] are also shown.

Channel	$N^{\rm net}_{\rm data}$	$\epsilon(\%)$	$\mathcal{B}_{\rm measured}(\times 10^{-4})$	$\mathcal{B}_{\rm PDG}(\times 10^{-4})$
$\chi_{c0} \to \omega\omega$	17458 ± 178	7.94 ± 0.24	$10.66 \pm 0.11_{\rm stat} \pm 0.57_{\rm syst}$	$9.7 \pm 1.1_{\rm tot}$
$\chi_{c1} \to \omega\omega$	11674 ± 128	8.83 ± 0.26	$6.43 \pm 0.07_{\rm stat} \pm 0.31_{\rm syst}$	$5.7 \pm 0.7_{\rm tot}$
$\chi_{c2} \to \omega\omega$	14276 ± 135	8.13 ± 0.25	$8.75 \pm 0.08_{\rm stat} \pm 0.42_{\rm syst}$	$8.4 \pm 1.9_{\rm tot}$
$\chi_{c0} \to \omega\phi$	1893 ± 51	13.93 ± 0.31	$1.18 \pm 0.03_{\rm stat} \pm 0.07_{\rm syst}$	$1.41 \pm 0.13_{\rm tot}$
$\chi_{c1} \to \omega\phi$	356 ± 26	15.27 ± 0.32	$0.20 \pm 0.02_{\rm stat} \pm 0.01_{\rm syst}$	$0.27 \pm 0.04_{\rm tot}$
$\chi_{c2} \to \omega\phi$	151 ± 17	14.18 ± 0.31	$0.10 \pm 0.01_{\rm stat} \pm 0.01_{\rm syst}$	$0.10 \pm 0.03_{\rm tot}$

where $\hat{S}$ is associated with the nominal efficiency, σ_S is its multiplicative systematic uncertainty, and $\mathcal{L}(N)$ is the likelihood distribution obtained from fitting the likelihood of the signal yields as shown in Fig. 10.

VII. RESULT AND SUMMARY

Using $(2712 \pm 14) \times 10^6$ $\psi(2S)$ events collected by the BESIII detector, we search for the hadronic decays $\eta_c(2S) \to \omega\omega$ and $\eta_c(2S) \to \omega\phi$ via the $\psi(2S) \to \gamma\eta_c(2S)$ process, and update the branching fractions of the $\chi_{cJ} \to \omega\omega$ and $\chi_{cJ} \to \omega\phi$ decays.

The upper limits of the product branching fractions of $\psi(2S) \to \gamma\eta_c(2S), \eta_c(2S) \to VV$ at the 90% C. are determined using

$$\mathcal{B}(\psi(2S) \to \gamma\eta_c(2S), \eta_c(2S) \to VV) < \frac{N^{\rm up}_{\rm sig}}{N^{\rm tot}_{\psi(2S)} \cdot \prod_i \mathcal{B}_i \cdot \epsilon}, \tag{6}$$

where $N^{\rm tot}_{\psi(2S)}$ is the total number of $\psi(2S)$ events, $\mathcal{B}_i$ are the branching fractions taken from the PDG [25], ϵ is the detection efficiency, which is $(6.78 \pm 0.23)\%$ for the $\gamma\omega\omega$ mode and $(12.10 \pm 0.29)\%$ for the $\gamma\omega\phi$ mode, and $N^{\rm up}_{\rm sig}$ is the upper limit of the number of signal events, which are 149.0 and 26.3 for the $\omega\omega$ and $\omega\phi$ modes, respectively. The branching fraction of $\psi(2S) \to \gamma\eta_c(2S)$ is not divided out, $\mathcal{B}(\psi(2S) \to \gamma\eta_c(2S)) = (5.2^{+2.0}_{-1.5}) \times 10^{-4}$ [42], as it is with large uncertainty. Thus, the upper limits of the product branching fractions of $\psi(2S) \to \gamma\eta_c(2S), \eta_c(2S) \to \omega\omega$ and $\psi(2S) \to \gamma\eta_c(2S), \eta_c(2S) \to \omega\phi$ are 1.04×10^{-6} and 1.85×10^{-7} at the 90% CL, respectively.

The branching fractions of $\eta_c(2S)/\chi_{cJ}(1P) \to \omega\omega$ and $\chi_{cJ}(1P) \to \omega\phi$ are calculated by

$$\mathcal{B}(\eta_c(2S)/\chi_{cJ} \to VV) = \frac{N^{\rm net}_{\rm data}}{N^{\rm tot}_{\psi(2S)} \cdot \prod_i \mathcal{B}_i \cdot \epsilon}, \tag{7}$$

where $N^{\rm net}_{\rm data}$ represents the number of signal events.

The branching fractions of $\eta_c(2S) \to VV$ decays are determined to be $\mathcal{B}(\eta_c(2S) \to \omega\omega) = (5.93 \pm 3.57({\rm stat}) \pm 6.57({\rm syst})) \times 10^{-4}$ and $\mathcal{B}(\eta_c(2S) \to \omega\phi) = (8.11 \pm 4.34({\rm stat}) \pm 12.03({\rm syst})) \times 10^{-5}$. The statistical significances of the $\eta_c(2S) \to \omega\omega$ and $\eta_c(2S) \to \omega\phi$ are 1.4σ and 1.1σ after considering systematic uncertainties, respectively. Combining our branching fraction of $\eta_c(2S) \to \omega\omega$ and that of $\eta_c(1S) \to \omega\omega$ [12], we calculate the branching fraction ratio to be

$$\frac{\mathcal{B}(\eta_c(2S) \to \omega\omega)}{\mathcal{B}(\eta_c(1S) \to \omega\omega)} = 0.36^{+0.48}_{-0.36}. \tag{8}$$

The precision of the current measurement does not allow to distinguish between the theoretical predictions of the three models [8–10].

For the branching fractions of $\chi_{cJ} \to VV$, the detection efficiencies in Eq. (7) are determined with the same fit procedure used in data. The peaking contributions estimated using the 2D sideband regions are subtracted. Table IV lists the detection efficiencies and calculated branching fractions. The $\chi_{c2} \to \omega\phi$ decay is observed with a statistical significance greater than 10σ. The measured branching fractions of the χ_{cJ} decays are consistent with the world average values [25], with precision improved by at least a factor of two. These measurements provide better constraints for the theoretical models used to explain the decay dynamics of charmonium states.

ACKNOWLEDGMENTS

The BESIII Collaboration thanks the staff of BEPCII and the IHEP computing center for their strong support. This work is supported in part by National Key R&D Program of China under Contracts No. 2020YFA0406300, No. 2020YFA0406400, No. 2023YFA1606000; National Natural Science Foundation of China (NSFC) under Contracts No. 12375070, No. 11635010, No. 11735014, No. 11935015, No. 11935016, No. 11935018, No. 12025502, No. 12035009, No. 12035013, No. 12061131003, No. 12192260, No. 12192261, No. 12192262, No. 12192263, No. 12192264, No. 12192265, No. 12221005, No. 12225509, No. 12235017, No. 12361141819; the Chinese Academy of Sciences (CAS) Large-Scale Scientific Facility Program; the CAS Center for Excellence in Particle Physics (CCEPP); Joint Large-Scale Scientific Facility Funds of the NSFC and CAS under Contracts No. U2032108, No. U1832207; Shanghai Leading Talent Program of Eastern Talent Plan under Contract No. JLH5913002; 100 Talents Program of CAS; The Institute of Nuclear and Particle Physics (INPAC) and Shanghai Key Laboratory for Particle Physics and Cosmology; German Research Foundation DFG under Contracts No. 455635585, No. FOR5327, No. GRK 2149; Istituto Nazionale di Fisica Nucleare, Italy; Ministry of Development of Turkey under Contract No. DPT2006K-120470; National Research Foundation of Korea under Contract No. NRF-2022R1A2C1092335; National Science and Technology fund of Mongolia; National Science Research and Innovation Fund (NSRF) via the Program Management Unit for Human Resources & Institutional Development, Research and Innovation of Thailand under Contract No. B16F640076; Polish National Science Centre under Contract No. 2019/35/O/ST2/02907; The Swedish Research Council; U.S. Department of Energy under Contract No. DE-FG02-05ER41374.

[1] N. Brambilla, S. Eidelman, B. K. Heltsley, R. Vogt, G. T. Bodwin, E. Eichten, A. D. Frawley, A. B. Meyer, R. E. Mitchell, V. Papadimitriou *et al.*, Eur. Phys. J. C **71**, 1534 (2011).
[2] S. J. Brodsky and G. P. Lepage, Phys. Rev. D **24**, 2848 (1981).
[3] V. L. Chernyak and A. R. Zhitnitsky, Nucl. Phys. **B201**, 492 (1982); **B214**, 547(E) (1983); V. L. Chernyak, A. R. Zhitnitsky, and I. R. Zhitnitsky, Nucl. Phys. **B204**, 477 (1982); **B214**, 547(E) (1983).
[4] V. L. Chernyak and A. R. Zhitnitsky, Phys. Rep. **112**, 173 (1984).
[5] P. Sun, G. Hao, and C. F. Qiao, Phys. Lett. B **702**, 49 (2011).
[6] Q. Zhao, Phys. Lett. B **636**, 197 (2006).
[7] T. Feldmann and P. Kroll, Phys. Rev. D **62**, 074006 (2000).
[8] H. Q. Zhou, R. G. Ping, and B. S. Zou, Phys. Rev. D **71**, 114002 (2005).
[9] M. Anselmino, M. Genovese, and E. Predazzi, Phys. Rev. D **44**, 1597 (1991).
[10] K. T. Chao, Y. F. Gu, and S. F. Tuan, Commun. Theor. Phys. **25**, 471 (1996).
[11] H. Wang and C. Z. Yuan, Chin. Phys. C **46**, 071001 (2022).
[12] Z. Q. Liu *et al.* (Belle Collaboration), Phys. Rev. Lett. **108**, 232001 (2012).
[13] M. Ablikim *et al.* (BESIII Collaboration), Phys. Rev. D **95**, 092004 (2017).
[14] M. Ablikim *et al.* (BESII Collaboration), Phys. Rev. Lett. **107**, 092001 (2011).
[15] H. Q. Zhou, R. G. Ping, and B. S. Zou, Phys. Lett. B **611**, 123 (2005); M. Ablikim *et al.* (BESII Collaboration), Phys. Rev. Lett. **107**, 092001 (2011).
[16] M. Ablikim *et al.* (BESIII Collaboration), Phys. Rev. D **99**, 012015 (2019).
[17] M. Ablikim *et al.* (BESIII Collaboration), Chin. Phys. C **48**, 093001 (2024).
[18] M. Ablikim *et al.* (BESIII Collaboration), Nucl. Instrum. Methods Phys. Res., Sect. A **614**, 345 (2010).
[19] C. H. Yu *et al.*, in *Proceedings of IPAC 2016* (JACoW, Geneva, Switzerland, 2016), https://accelconf.web.cern.ch/ipac2016/doi/JACoW-IPAC2016-TUYA01.html.
[20] X. Li, Y. Sun, C. Li, Z. Liu, Y. Heng, M. Shao, X. Wang, Z. Wu, P. Cao, M. Chen *et al.*, Radiat. Detect. Technol. Methods **1**, 13 (2017); Y. X. Guo, S. S. Sun, F. F. An, R. X. Yang, M. Zhou, Z. Wu, H. L. Dai, Y. K. Heng, C. Li, Z. Y. Deng *et al.*, Radiat. Detect. Technol. Methods **1**, 15 (2017).
[21] S. Agostinelli *et al.* (Geant4 Collaboration), Nucl. Instrum. Methods Phys. Res., Sect. A **506**, 250 (2003).
[22] K. X. Huang, Z. J. Li, Z. Qian, J. Zhu, H. Y. Li, Y. M. Zhang, S. S. Sun, and Z. Y. You, Nucl. Sci. Tech. **33**, 142 (2022).
[23] S. Jadach, B. F. L. Ward, and Z. Was, Phys. Rev. D **63**, 113009 (2001); Comput. Phys. Commun. **130**, 260 (2000).
[24] D. J. Lange, Nucl. Instrum. Methods Phys. Res., Sect. A **462**, 152 (2001); R. G. Ping, Chin. Phys. C **32**, 599 (2008).
[25] R. L. Workman *et al.* (Particle Data Group), Prog. Theor. Exp. Phys. **2022**, 083C01 (2022).
[26] J. C. Chen, G. S. Huang, X. R. Qi, D. H. Zhang, and Y. S. Zhu, Phys. Rev. D **62**, 034003 (2000); R. L. Yang, R. G. Ping, and H. Chen, Chin. Phys. Lett. **31**, 061301 (2014).
[27] E. Barberio, B. van Eijk, and Z. Was, Comput. Phys. Commun. **66**, 115 (1991).
[28] W. M. Tanenbaum, M. S. Alam, A. Boyarski, M. Breidenbach, G. J. Feldman, G. Hanson, J. Jaros, R. R. Larsen, D. Luke, V. Luth *et al.*, Phys. Rev. D **17**, 1731 (1978).
[29] G. Punzi, in PHYSTAT 2003 (SLAC, 2003), arXiv:physics/0308063v2.
[30] M. Ablikim *et al.* (BESIII Collaboration), Phys. Rev. D **106**, 032014 (2022).
[31] V. V. Anashin, V. M. Aulchenko, E. M. Baldin, A. K. Barladyan, A. Y. Barnyakov, M. Y. Barnyakov, S. E. Baru, I. Y. Basok, I. V. Bedny, O. L. Beloborodova *et al.*, Int. J. Mod. Phys. Conf. Ser. **02**, 188 (2011).
[32] H. Albrecht *et al.* (ARGUS Collaboration), Phys. Lett. B **241**, 278 (1990).
[33] K. S. Cranmer, Comput. Phys. Commun. **136**, 198 (2001).
[34] S. S. Wilks, Ann. Math. Stat. **9**, 60 (1938).
[35] M. Ablikim *et al.* (BESIII Collaboration), Phys. Rev. D **83**, 112005 (2011).
[36] M. Ablikim *et al.* (BESIII Collaboration), Phys. Rev. D **102**, 092006 (2020).
[37] M. Ablikim *et al.* (BESIII Collaboration), Phys. Rev. Lett. **105**, 261801 (2010).
[38] M. Ablikim *et al.* (BESIII Collaboration), Phys. Rev. D **87**, 012002 (2013).

[39] R. E. Mitchell *et al.* (CLEO Collaboration), Phys. Rev. Lett. **102**, 011801 (2009); **106**, 159903(E) (2011).
[40] R. Brun and F. Rademakers, Nucl. Instrum. Methods Phys. Res., Sect. A **389**, 81 (1997).
[41] K. Stenson, arXiv:physics/0605236.
[42] M. Ablikim *et al.* (BESIII Collaboration), Phys. Rev. D **109**, 032004 (2024).

M. Ablikim,[1] M. N. Achasov,[4,c] P. Adlarson,[75] O. Afedulidis,[3] X. C. Ai,[80] R. Aliberti,[35] A. Amoroso,[74a,74c] Q. An,[71,58,a] Y. Bai,[57] O. Bakina,[36] I. Balossino,[29a] Y. Ban,[46,h] H.-R. Bao,[63] V. Batozskaya,[1,44] K. Begzsuren,[32] N. Berger,[35] M. Berlowski,[44] M. Bertani,[28a] D. Bettoni,[29a] F. Bianchi,[74a,74c] E. Bianco,[74a,74c] A. Bortone,[74a,74c] I. Boyko,[36] R. A. Briere,[5] A. Brueggemann,[68] H. Cai,[76] X. Cai,[1,58] A. Calcaterra,[28a] G. F. Cao,[1,63] N. Cao,[1,63] S. A. Cetin,[62a] J. F. Chang,[1,58] G. R. Che,[43] G. Chelkov,[36,b] C. Chen,[43] C. H. Chen,[9] Chao Chen,[55] G. Chen,[1] H. S. Chen,[1,63] H. Y. Chen,[20] M. L. Chen,[1,58,63] S. J. Chen,[42] S. L. Chen,[45] S. M. Chen,[61] T. Chen,[1,63] X. R. Chen,[31,63] X. T. Chen,[1,63] Y. B. Chen,[1,58] Y. Q. Chen,[34] Z. J. Chen,[25,i] Z. Y. Chen,[1,63] S. K. Choi,[10] X. Chu,[12,g] G. Cibinetto,[29a] F. Cossio,[74c] J. J. Cui,[50] H. L. Dai,[1,58] J. P. Dai,[78] A. Dbeyssi,[18] R. E. de Boer,[3] D. Dedovich,[36] C. Q. Deng,[72] Z. Y. Deng,[1] A. Denig,[35] I. Denysenko,[36] M. Destefanis,[74a,74c] F. De Mori,[74a,74c] B. Ding,[66,1] X. X. Ding,[46,h] Y. Ding,[34] Y. Ding,[40] J. Dong,[1,58] L. Y. Dong,[1,63] M. Y. Dong,[1,58,63] X. Dong,[76] M. C. Du,[1] S. X. Du,[80] Y. Y. Duan,[55] Z. H. Duan,[42] P. Egorov,[36,b] Y. H. Fan,[45] J. Fang,[59] J. Fang,[1,58] S. S. Fang,[1,63] W. X. Fang,[1] Y. Fang,[1] Y. Q. Fang,[1,58] R. Farinelli,[29a] L. Fava,[74b,74c] F. Feldbauer,[3] G. Felici,[28a] C. Q. Feng,[71,58] J. H. Feng,[59] Y. T. Feng,[71,58] M. Fritsch,[3] C. D. Fu,[1] J. L. Fu,[63] Y. W. Fu,[1,63] H. Gao,[63] X. B. Gao,[41] Y. N. Gao,[46,h] Yang Gao,[71,58] S. Garbolino,[74c] I. Garzia,[29a,29b] L. Ge,[80] P. T. Ge,[76] Z. W. Ge,[42] C. Geng,[59] E. M. Gersabeck,[67] A. Gilman,[69] K. Goetzen,[13] L. Gong,[40] W. X. Gong,[1,58] W. Gradl,[35] S. Gramigna,[29a,29b] M. Greco,[74a,74c] M. H. Gu,[1,58] Y. T. Gu,[15] C. Y. Guan,[1,63] A. Q. Guo,[31,63] L. B. Guo,[41] M. J. Guo,[50] R. P. Guo,[49] Y. P. Guo,[12,g] A. Guskov,[36,b] J. Gutierrez,[27] K. L. Han,[63] T. T. Han,[1] F. Hanisch,[3] X. Q. Hao,[19] F. A. Harris,[65] K. K. He,[55] K. L. He,[1,63] F. H. Heinsius,[3] C. H. Heinz,[35] Y. K. Heng,[1,58,63] C. Herold,[60] T. Holtmann,[3] P. C. Hong,[34] G. Y. Hou,[1,63] X. T. Hou,[1,63] Y. R. Hou,[63] Z. L. Hou,[1] B. Y. Hu,[59] H. M. Hu,[1,63] J. F. Hu,[56,j] S. L. Hu,[12,g] T. Hu,[1,58,63] Y. Hu,[1] G. S. Huang,[71,58] K. X. Huang,[59] L. Q. Huang,[31,63] X. T. Huang,[50] Y. P. Huang,[1] Y. S. Huang,[59] T. Hussain,[73] F. Hölzken,[3] N. Hüsken,[35] N. in der Wiesche,[68] J. Jackson,[27] S. Janchiv,[32] J. H. Jeong,[10] Q. Ji,[1] Q. P. Ji,[19] W. Ji,[1,63] X. B. Ji,[1,63] X. L. Ji,[1,58] Y. Y. Ji,[50] X. Q. Jia,[50] Z. K. Jia,[71,58] D. Jiang,[1,63] H. B. Jiang,[76] P. C. Jiang,[46,h] S. S. Jiang,[39] T. J. Jiang,[16] X. S. Jiang,[1,58,63] Y. Jiang,[63] J. B. Jiao,[50] J. K. Jiao,[34] Z. Jiao,[23] S. Jin,[42] Y. Jin,[66] M. Q. Jing,[1,63] X. M. Jing,[63] T. Johansson,[75] S. Kabana,[33] N. Kalantar-Nayestanaki,[64] X. L. Kang,[9] X. S. Kang,[40] M. Kavatsyuk,[64] B. C. Ke,[80] V. Khachatryan,[27] A. Khoukaz,[68] R. Kiuchi,[1] O. B. Kolcu,[62a] B. Kopf,[3] M. Kuessner,[3] X. Kui,[1,63] N. Kumar,[26] A. Kupsc,[44,75] W. Kühn,[37] J. J. Lane,[67] L. Lavezzi,[74a,74c] T. T. Lei,[71,58] Z. H. Lei,[71,58] M. Lellmann,[35] T. Lenz,[35] C. Li,[47] C. Li,[43] C. H. Li,[39] Cheng Li,[71,58] D. M. Li,[80] F. Li,[1,58] G. Li,[1] H. B. Li,[1,63] H. J. Li,[19] H. N. Li,[56,j] Hui Li,[43] J. R. Li,[61] J. S. Li,[59] K. Li,[1] L. J. Li,[1,63] L. K. Li,[1] Lei Li,[48] M. H. Li,[43] P. R. Li,[38,k,l] Q. M. Li,[1,63] Q. X. Li,[50] R. Li,[17,31] S. X. Li,[12] T. Li,[50] W. D. Li,[1,63] W. G. Li,[1,a] X. Li,[1,63] X. H. Li,[71,58] X. L. Li,[50] X. Y. Li,[1,63] X. Z. Li,[59] Y. G. Li,[46,h] Z. J. Li,[59] Z. Y. Li,[78] C. Liang,[42] H. Liang,[1,63] H. Liang,[71,58] Y. F. Liang,[54] Y. T. Liang,[31,63] G. R. Liao,[14] Y. P. Liao,[1,63] J. Libby,[26] A. Limphirat,[60] C. C. Lin,[55] D. X. Lin,[31,63] T. Lin,[1] B. J. Liu,[1] B. X. Liu,[76] C. Liu,[34] C. X. Liu,[1] F. Liu,[1] F. H. Liu,[53] Feng Liu,[6] G. M. Liu,[56,j] H. Liu,[38,k,l] H. B. Liu,[15] H. H. Liu,[1] H. M. Liu,[1,63] Huihui Liu,[21] J. B. Liu,[71,58] J. Y. Liu,[1,63] K. Liu,[38,k,l] K. Y. Liu,[40] Ke Liu,[22] L. Liu,[71,58] L. C. Liu,[43] Lu Liu,[43] M. H. Liu,[12,g] P. L. Liu,[1] Q. Liu,[63] S. B. Liu,[71,58] T. Liu,[12,g] W. K. Liu,[43] W. M. Liu,[71,58] X. Liu,[38,k,l] X. Liu,[39] Y. Liu,[80] Y. Liu,[38,k,l] Y. B. Liu,[43] Z. A. Liu,[1,58,63] Z. D. Liu,[9] Z. Q. Liu,[50] X. C. Lou,[1,58,63] F. X. Lu,[59] H. J. Lu,[23] J. G. Lu,[1,58] X. L. Lu,[1] Y. Lu,[7] Y. P. Lu,[1,58] Z. H. Lu,[1,63] C. L. Luo,[41] J. R. Luo,[59] M. X. Luo,[79] T. Luo,[12,g] X. L. Luo,[1,58] X. R. Lyu,[63] Y. F. Lyu,[43] F. C. Ma,[40] H. Ma,[78] H. L. Ma,[1] J. L. Ma,[1,63] L. L. Ma,[50] M. M. Ma,[1,63] Q. M. Ma,[1] R. Q. Ma,[1,63] T. Ma,[71,58] X. T. Ma,[1,63] X. Y. Ma,[1,58] Y. Ma,[46,h] Y. M. Ma,[31] F. E. Maas,[18] M. Maggiora,[74a,74c] S. Malde,[69] Y. J. Mao,[46,h] Z. P. Mao,[1] S. Marcello,[74a,74c] Z. X. Meng,[66] J. G. Messchendorp,[13,64] G. Mezzadri,[29a] H. Miao,[1,63] T. J. Min,[42] R. E. Mitchell,[27] X. H. Mo,[1,58,63] B. Moses,[27] N. Yu. Muchnoi,[4,c] J. Muskalla,[35] Y. Nefedov,[36] F. Nerling,[18,e] L. S. Nie,[20] I. B. Nikolaev,[4,c] Z. Ning,[1,58] S. Nisar,[11,m] Q. L. Niu,[38,k,l] W. D. Niu,[55] Y. Niu,[50] S. L. Olsen,[63] Q. Ouyang,[1,58,63] S. Pacetti,[28b,28c] X. Pan,[55] Y. Pan,[57] A. Pathak,[34] Y. P. Pei,[71,58] M. Pelizaeus,[3] H. P. Peng,[71,58] Y. Y. Peng,[38,k,l] K. Peters,[13,e] J. L. Ping,[41] R. G. Ping,[1,63] S. Plura,[35] V. Prasad,[33] F. Z. Qi,[1] H. Qi,[71,58] H. R. Qi,[61] M. Qi,[42] T. Y. Qi,[12,g] S. Qian,[1,58] W. B. Qian,[63] C. F. Qiao,[63] X. K. Qiao,[80] J. J. Qin,[72] L. Q. Qin,[14] L. Y. Qin,[71,58] X. P. Qin,[12,g] X. S. Qin,[50] Z. H. Qin,[1,58] J. F. Qiu,[1] Z. H. Qu,[72] C. F. Redmer,[35] K. J. Ren,[39] A. Rivetti,[74c] M. Rolo,[74c] G. Rong,[1,63] Ch. Rosner,[18] S. N. Ruan,[43]

N. Salone,[44] A. Sarantsev,[36,d] Y. Schelhaas,[35] K. Schoenning,[75] M. Scodeggio,[29a] K. Y. Shan,[12,g] W. Shan,[24] X. Y. Shan,[71,58] Z. J. Shang,[38,k,l] J. F. Shangguan,[16] L. G. Shao,[1,63] M. Shao,[71,58] C. P. Shen,[12,g] H. F. Shen,[1,8] W. H. Shen,[63] X. Y. Shen,[1,63] B. A. Shi,[63] H. Shi,[71,58] H. C. Shi,[71,58] J. L. Shi,[12,g] J. Y. Shi,[1] Q. Q. Shi,[55] S. Y. Shi,[72] X. Shi,[1,58] J. J. Song,[19] T. Z. Song,[59] W. M. Song,[34,1] Y. J. Song,[12,g] Y. X. Song,[46,h,n] S. Sosio,[74a,74c] S. Spataro,[74a,74c] F. Stieler,[35] Y. J. Su,[63] G. B. Sun,[76] G. X. Sun,[1] H. Sun,[63] H. K. Sun,[1] J. F. Sun,[19] K. Sun,[61] L. Sun,[76] S. S. Sun,[1,63] T. Sun,[51,f] W. Y. Sun,[34] Y. Sun,[9] Y. J. Sun,[71,58] Y. Z. Sun,[1] Z. Q. Sun,[1,63] Z. T. Sun,[50] C. J. Tang,[54] G. Y. Tang,[1] J. Tang,[59] M. Tang,[71,58] Y. A. Tang,[76] L. Y. Tao,[72] Q. T. Tao,[25,i] M. Tat,[69] J. X. Teng,[71,58] V. Thoren,[75] W. H. Tian,[59] Y. Tian,[31,63] Z. F. Tian,[76] I. Uman,[62b] Y. Wan,[55] S. J. Wang,[50] B. Wang,[1] B. L. Wang,[63] Bo Wang,[71,58] D. Y. Wang,[46,h] F. Wang,[72] H. J. Wang,[38,k,l] J. J. Wang,[76] J. P. Wang,[50] K. Wang,[1,58] L. L. Wang,[1] M. Wang,[50] N. Y. Wang,[63] S. Wang,[12,g] S. Wang,[38,k,l] T. Wang,[12,g] T. J. Wang,[43] W. Wang,[59] W. Wang,[72] W. P. Wang,[35,71,o] X. Wang,[46,h] X. F. Wang,[38,k,l] X. J. Wang,[39] X. L. Wang,[12,g] X. N. Wang,[1] Y. Wang,[61] Y. D. Wang,[45] Y. F. Wang,[1,58,63] Y. L. Wang,[19] Y. N. Wang,[45] Y. Q. Wang,[1] Yaqian Wang,[17] Yi Wang,[61] Z. Wang,[1,58] Z. L. Wang,[72] Z. Y. Wang,[1,63] Ziyi Wang,[63] D. H. Wei,[14] F. Weidner,[68] S. P. Wen,[1] Y. R. Wen,[39] U. Wiedner,[3] G. Wilkinson,[69] M. Wolke,[75] L. Wollenberg,[3] C. Wu,[39] J. F. Wu,[1,8] L. H. Wu,[1] L. J. Wu,[1,63] X. Wu,[12,g] X. H. Wu,[34] Y. Wu,[71,58] Y. H. Wu,[55] Y. J. Wu,[31] Z. Wu,[1,58] L. Xia,[71,58] X. M. Xian,[39] B. H. Xiang,[1,63] T. Xiang,[46,h] D. Xiao,[38,k,l] G. Y. Xiao,[42] S. Y. Xiao,[1] Y. L. Xiao,[12,g] Z. J. Xiao,[41] C. Xie,[42] X. H. Xie,[46,h] Y. Xie,[50] Y. G. Xie,[1,58] Y. H. Xie,[6] Z. P. Xie,[71,58] T. Y. Xing,[1,63] C. F. Xu,[1,63] C. J. Xu,[59] G. F. Xu,[1] H. Y. Xu,[66,2,p] M. Xu,[71,58] Q. J. Xu,[16] Q. N. Xu,[30] W. Xu,[1] W. L. Xu,[66] X. P. Xu,[55] Y. C. Xu,[77] Z. S. Xu,[63] F. Yan,[12,g] L. Yan,[12,g] W. B. Yan,[71,58] W. C. Yan,[80] X. Q. Yan,[1] H. J. Yang,[51,f] H. L. Yang,[34] H. X. Yang,[1] T. Yang,[1] Y. Yang,[12,g] Y. F. Yang,[1,63] Y. F. Yang,[43] Y. X. Yang,[1,63] Z. W. Yang,[38,k,l] Z. P. Yao,[50] M. Ye,[1,58] M. H. Ye,[8] J. H. Yin,[1] Z. Y. You,[59] B. X. Yu,[1,58,63] C. X. Yu,[43] G. Yu,[1,63] J. S. Yu,[25,i] T. Yu,[72] X. D. Yu,[46,h] Y. C. Yu,[80] C. Z. Yuan,[1,63] J. Yuan,[34] J. Yuan,[45] L. Yuan,[2] S. C. Yuan,[1,63] Y. Yuan,[1,63] Z. Y. Yuan,[59] C. X. Yue,[39] A. A. Zafar,[73] F. R. Zeng,[50] S. H. Zeng,[72] X. Zeng,[12,g] Y. Zeng,[25,i] Y. J. Zeng,[59] Y. J. Zeng,[1,63] X. Y. Zhai,[34] Y. C. Zhai,[50] Y. H. Zhan,[59] A. Q. Zhang,[1,63] B. L. Zhang,[1,63] B. X. Zhang,[1] D. H. Zhang,[43] G. Y. Zhang,[19] H. Zhang,[80] H. Zhang,[71,58] H. C. Zhang,[1,58,63] H. H. Zhang,[34] H. H. Zhang,[59] H. Q. Zhang,[1,58,63] H. R. Zhang,[71,58] H. Y. Zhang,[1,58] J. Zhang,[80] J. Zhang,[59] J. J. Zhang,[52] J. L. Zhang,[20] J. Q. Zhang,[41] J. S. Zhang,[12,g] J. W. Zhang,[1,58,63] J. X. Zhang,[38,k,l] J. Y. Zhang,[1] J. Z. Zhang,[1,63] Jianyu Zhang,[63] L. M. Zhang,[61] Lei Zhang,[42] P. Zhang,[1,63] Q. Y. Zhang,[34] R. Y. Zhang,[38,k,l] S. H. Zhang,[1,63] Shulei Zhang,[25,i] X. D. Zhang,[45] X. M. Zhang,[1] X. Y. Zhang,[50] Y. Zhang,[72] Y. Zhang,[1] Y. T. Zhang,[80] Y. H. Zhang,[1,58] Y. M. Zhang,[39] Yan Zhang,[71,58] Z. D. Zhang,[1] Z. H. Zhang,[1] Z. L. Zhang,[34] Z. Y. Zhang,[76] Z. Y. Zhang,[43] Z. Z. Zhang,[45] G. Zhao,[1] J. Y. Zhao,[1,63] J. Z. Zhao,[1,58] L. Zhao,[1] Lei Zhao,[71,58] M. G. Zhao,[43] N. Zhao,[78] R. P. Zhao,[63] S. J. Zhao,[80] Y. B. Zhao,[1,58] Y. X. Zhao,[31,63] Z. G. Zhao,[71,58] A. Zhemchugov,[36,b] B. Zheng,[72] B. M. Zheng,[34] J. P. Zheng,[1,58] W. J. Zheng,[1,63] Y. H. Zheng,[63] B. Zhong,[41] X. Zhong,[59] H. Zhou,[50] J. Y. Zhou,[34] L. P. Zhou,[1,63] S. Zhou,[6] X. Zhou,[76] X. K. Zhou,[6] X. R. Zhou,[71,58] X. Y. Zhou,[39] Y. Z. Zhou,[12,g] J. Zhu,[43] K. Zhu,[1] K. J. Zhu,[1,58,63] K. S. Zhu,[12,g] L. Zhu,[34] L. X. Zhu,[63] S. H. Zhu,[70] T. J. Zhu,[12,g] W. D. Zhu,[41] Y. C. Zhu,[71,58] Z. A. Zhu,[1,63] J. H. Zou,[1] and J. Zu[71,58]

(BESIII Collaboration)

[1]*Institute of High Energy Physics, Beijing 100049, People's Republic of China*
[2]*Beihang University, Beijing 100191, People's Republic of China*
[3]*Bochum Ruhr-University, D-44780 Bochum, Germany*
[4]*Budker Institute of Nuclear Physics SB RAS (BINP), Novosibirsk 630090, Russia*
[5]*Carnegie Mellon University, Pittsburgh, Pennsylvania 15213, USA*
[6]*Central China Normal University, Wuhan 430079, People's Republic of China*
[7]*Central South University, Changsha 410083, People's Republic of China*
[8]*China Center of Advanced Science and Technology, Beijing 100190, People's Republic of China*
[9]*China University of Geosciences, Wuhan 430074, People's Republic of China*
[10]*Chung-Ang University, Seoul, 06974, Republic of Korea*
[11]*COMSATS University Islamabad, Lahore Campus, Defence Road, Off Raiwind Road, 54000 Lahore, Pakistan*
[12]*Fudan University, Shanghai 200433, People's Republic of China*
[13]*GSI Helmholtzcentre for Heavy Ion Research GmbH, D-64291 Darmstadt, Germany*
[14]*Guangxi Normal University, Guilin 541004, People's Republic of China*
[15]*Guangxi University, Nanning 530004, People's Republic of China*
[16]*Hangzhou Normal University, Hangzhou 310036, People's Republic of China*

[17]*Hebei University, Baoding 071002, People's Republic of China*
[18]*Helmholtz Institute Mainz, Staudinger Weg 18, D-55099 Mainz, Germany*
[19]*Henan Normal University, Xinxiang 453007, People's Republic of China*
[20]*Henan University, Kaifeng 475004, People's Republic of China*
[21]*Henan University of Science and Technology, Luoyang 471003, People's Republic of China*
[22]*Henan University of Technology, Zhengzhou 450001, People's Republic of China*
[23]*Huangshan College, Huangshan 245000, People's Republic of China*
[24]*Hunan Normal University, Changsha 410081, People's Republic of China*
[25]*Hunan University, Changsha 410082, People's Republic of China*
[26]*Indian Institute of Technology Madras, Chennai 600036, India*
[27]*Indiana University, Bloomington, Indiana 47405, USA*
[28a]*INFN Laboratori Nazionali di Frascati, I-00044, Frascati, Italy*
[28b]*INFN Sezione di Perugia, I-06100, Perugia, Italy*
[28c]*University of Perugia, I-06100, Perugia, Italy*
[29a]*INFN Sezione di Ferrara, I-44122, Ferrara, Italy*
[29b]*University of Ferrara, I-44122, Ferrara, Italy*
[30]*Inner Mongolia University, Hohhot 010021, People's Republic of China*
[31]*Institute of Modern Physics, Lanzhou 730000, People's Republic of China*
[32]*Institute of Physics and Technology, Peace Avenue 54B, Ulaanbaatar 13330, Mongolia*
[33]*Instituto de Alta Investigación, Universidad de Tarapacá, Casilla 7D, Arica 1000000, Chile*
[34]*Jilin University, Changchun 130012, People's Republic of China*
[35]*Johannes Gutenberg University of Mainz, Johann-Joachim-Becher-Weg 45, D-55099 Mainz, Germany*
[36]*Joint Institute for Nuclear Research, 141980 Dubna, Moscow region, Russia*
[37]*Justus-Liebig-Universitaet Giessen, II. Physikalisches Institut, Heinrich-Buff-Ring 16, D-35392 Giessen, Germany*
[38]*Lanzhou University, Lanzhou 730000, People's Republic of China*
[39]*Liaoning Normal University, Dalian 116029, People's Republic of China*
[40]*Liaoning University, Shenyang 110036, People's Republic of China*
[41]*Nanjing Normal University, Nanjing 210023, People's Republic of China*
[42]*Nanjing University, Nanjing 210093, People's Republic of China*
[43]*Nankai University, Tianjin 300071, People's Republic of China*
[44]*National Centre for Nuclear Research, Warsaw 02-093, Poland*
[45]*North China Electric Power University, Beijing 102206, People's Republic of China*
[46]*Peking University, Beijing 100871, People's Republic of China*
[47]*Qufu Normal University, Qufu 273165, People's Republic of China*
[48]*Renmin University of China, Beijing 100872, People's Republic of China*
[49]*Shandong Normal University, Jinan 250014, People's Republic of China*
[50]*Shandong University, Jinan 250100, People's Republic of China*
[51]*Shanghai Jiao Tong University, Shanghai 200240, People's Republic of China*
[52]*Shanxi Normal University, Linfen 041004, People's Republic of China*
[53]*Shanxi University, Taiyuan 030006, People's Republic of China*
[54]*Sichuan University, Chengdu 610064, People's Republic of China*
[55]*Soochow University, Suzhou 215006, People's Republic of China*
[56]*South China Normal University, Guangzhou 510006, People's Republic of China*
[57]*Southeast University, Nanjing 211100, People's Republic of China*
[58]*State Key Laboratory of Particle Detection and Electronics, Beijing 100049, Hefei 230026, People's Republic of China*
[59]*Sun Yat-Sen University, Guangzhou 510275, People's Republic of China*
[60]*Suranaree University of Technology, University Avenue 111, Nakhon Ratchasima 30000, Thailand*
[61]*Tsinghua University, Beijing 100084, People's Republic of China*
[62a]*Turkish Accelerator Center Particle Factory Group, Istinye University, 34010, Istanbul, Turkey*
[62b]*Near East University, Nicosia, North Cyprus, 99138, Mersin 10, Turkey*
[63]*University of Chinese Academy of Sciences, Beijing 100049, People's Republic of China*
[64]*University of Groningen, NL-9747 AA Groningen, The Netherlands*
[65]*University of Hawaii, Honolulu, Hawaii 96822, USA*
[66]*University of Jinan, Jinan 250022, People's Republic of China*
[67]*University of Manchester, Oxford Road, Manchester, M13 9PL, United Kingdom*
[68]*University of Muenster, Wilhelm-Klemm-Strasse 9, 48149 Muenster, Germany*
[69]*University of Oxford, Keble Road, Oxford OX13RH, United Kingdom*
[70]*University of Science and Technology Liaoning, Anshan 114051, People's Republic of China*

[71]University of Science and Technology of China, Hefei 230026, People's Republic of China
[72]University of South China, Hengyang 421001, People's Republic of China
[73]University of the Punjab, Lahore-54590, Pakistan
[74a]University of Turin and INFN, University of Turin, I-10125, Turin, Italy
[74b]University of Eastern Piedmont, I-15121, Alessandria, Italy
[74c]INFN, I-10125, Turin, Italy
[75]Uppsala University, Box 516, SE-75120 Uppsala, Sweden
[76]Wuhan University, Wuhan 430072, People's Republic of China
[77]Yantai University, Yantai 264005, People's Republic of China
[78]Yunnan University, Kunming 650500, People's Republic of China
[79]Zhejiang University, Hangzhou 310027, People's Republic of China
[80]Zhengzhou University, Zhengzhou 450001, People's Republic of China

[a]Deceased.
[b]Also at the Moscow Institute of Physics and Technology, Moscow 141700, Russia.
[c]Also at the Novosibirsk State University, Novosibirsk, 630090, Russia.
[d]Also at the NRC "Kurchatov Institute," PNPI, 188300, Gatchina, Russia.
[e]Also at Goethe University Frankfurt, 60323 Frankfurt am Main, Germany.
[f]Also at Key Laboratory for Particle Physics, Astrophysics and Cosmology, Ministry of Education; Shanghai Key Laboratory for Particle Physics and Cosmology; Institute of Nuclear and Particle Physics, Shanghai 200240, People's Republic of China.
[g]Also at Key Laboratory of Nuclear Physics and Ion-beam Application (MOE) and Institute of Modern Physics, Fudan University, Shanghai 200443, People's Republic of China.
[h]Also at State Key Laboratory of Nuclear Physics and Technology, Peking University, Beijing 100871, People's Republic of China.
[i]Also at School of Physics and Electronics, Hunan University, Changsha 410082, China.
[j]Also at Guangdong Provincial Key Laboratory of Nuclear Science, Institute of Quantum Matter, South China Normal University, Guangzhou 510006, China.
[k]Also at MOE Frontiers Science Center for Rare Isotopes, Lanzhou University, Lanzhou 730000, People's Republic of China.
[l]Also at Lanzhou Center for Theoretical Physics, Lanzhou University, Lanzhou 730000, People's Republic of China.
[m]Also at the Department of Mathematical Sciences, IBA, Karachi 75270, Pakistan.
[n]Also at Ecole Polytechnique Federale de Lausanne (EPFL), CH-1015 Lausanne, Switzerland.
[o]Also at Helmholtz Institute Mainz, Staudinger Weg 18, D-55099 Mainz, Germany.
[p]Also at School of Physics, Beihang University, Beijing 100191, China.